



저작자표시-비영리-변경금지 2.0 대한민국

이용자는 아래의 조건을 따르는 경우에 한하여 자유롭게

- 이 저작물을 복제, 배포, 전송, 전시, 공연 및 방송할 수 있습니다.

다음과 같은 조건을 따라야 합니다:



저작자표시. 귀하는 원저작자를 표시하여야 합니다.



비영리. 귀하는 이 저작물을 영리 목적으로 이용할 수 없습니다.



변경금지. 귀하는 이 저작물을 개작, 변형 또는 가공할 수 없습니다.

- 귀하는, 이 저작물의 재이용이나 배포의 경우, 이 저작물에 적용된 이용허락조건을 명확하게 나타내어야 합니다.
- 저작권자로부터 별도의 허가를 받으면 이러한 조건들은 적용되지 않습니다.

저작권법에 따른 이용자의 권리는 위의 내용에 의하여 영향을 받지 않습니다.

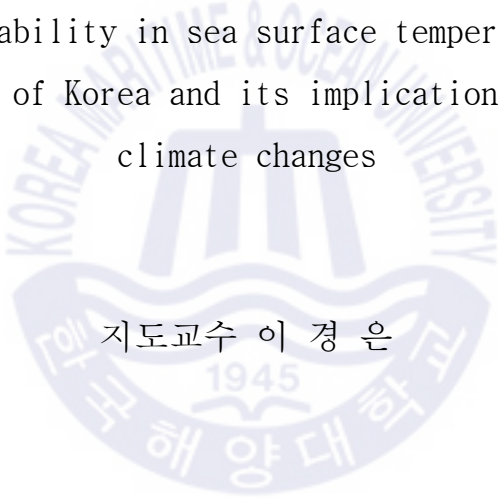
이것은 [이용허락규약\(Legal Code\)](#)을 이해하기 쉽게 요약한 것입니다.

[Disclaimer](#)

이학박사 학위논문

홀로세 한반도 서남해 연안  
표층수온변화와 동아시아 기후변화

Holocene variability in sea surface temperature off the  
southwest coast of Korea and its implications for East Asia  
climate changes



지도교수 이 경 은

2020년 2월

한국해양대학교 해양과학기술전문대학원

해양과학기술융합학과

배 시 응

본 논문을 배시웅의 이학박사 학위논문으로 인준함.

위원장 이 희 준 (인)

위 원 이 경 은 (인)

위 원 장 태 수 (인)

위 원 박 영 규 (인)

위 원 함 도 식 (인)

위 원 도 기 덕 (인)

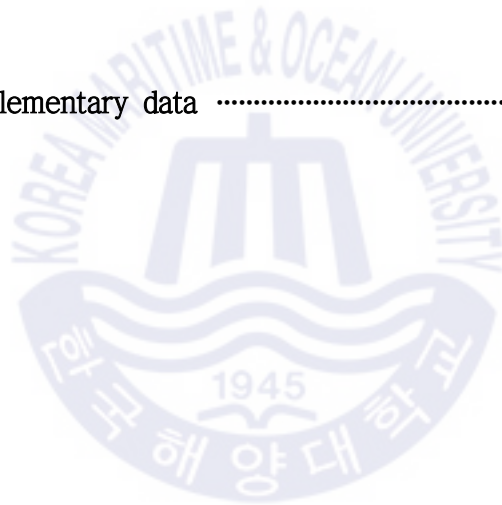
2019년 11월 19일

한국해양대학교 해양과학기술전문대학원

## Table of Contents

List of Tables .....	iii
List of Figures .....	iv
Abstract .....	viii
Chapter 1. Introduction .....	1
Chapter 2. Two long and pronounced cold periods 3,000–5,000 and 6,600–8,400 years B.P. in East Asia and the southward migration of the westerly jet	
2.1 Introduction .....	3
2.2 Geological and oceanographic settings .....	6
2.3 Materials and methods .....	9
2.4 Results .....	12
2.4.1 Core-top sediments .....	12
2.4.2 Deep-drilled core sediments .....	16
2.5 Discussion .....	18
2.5.1 Regional surface temperature changes .....	18
2.5.2 Potential factors affecting the SST changes .....	22
2.6 Conclusions .....	29
Chapter 3. Holocene centennial-scale variability in sea surface temperature in the southeast Yellow Sea	
3.1 Introduction .....	31
3.2 Materials and methods .....	32
3.3 Results .....	33

3.4 Discussion .....	37
3.4.1 Centennial variations in SST and solar activity .....	37
3.4.2 Validation of the centennial-scale SST variations .....	40
3.5 Conclusions .....	45
 Chapter 4. Conclusions .....	 46
 Acknowledgements .....	 47
 References .....	 48
 Appendix A. Supplementary data .....	 60



## List of Tables

Table 1. $^{14}\text{C}$ ages for core HMB-103 and HMB-102 and $^{210}\text{Pb}$ ages for core YS-C11 and YS-C04 .....	10
--	----



## List of Figures

**Fig. 1.** (a) Distribution of Holocene mud deposits (dark gray shading) and surface currents in the Yellow Sea and East China Sea. Blue (red) arrow represents cold (warm) current. Dashed arrow indicates seasonally varying current. Orange dashed line represents the thermohaline front. TWC, Tsushima Warm Current; CWC, Cheju Warm Current; YSWC, Yellow Sea Warm Current; KCC, Korean Coastal Current; CCC, Chinese Coastal Current; CDW, Changjiang Diluted Water. (b) Bathymetric map of the study area (contours in m) and core locations. The Heuksan Mud Belt (HMB) is marked by yellow shading. Red and black square indicates the location of the two deep-drilled cores (HMB-102, HMB-103) and piston cores (YS-C11, YS-C04) (Park et al., 2000), respectively. Blue dot indicates the location of the core-top sediment. Black triangle indicates the Heuksando Weather Station and Chilbaldo Buoy Station of the Korea Meteorological Administration. Green zigzag line represents the distribution of the tidal front. .... 5

**Fig. 2.** (a) Monthly fluctuation (1998 and 2018) and (b) 5-year average values of the SST at the Chilbaldo Buoy Station (red) and SAT at the Heuksando Weather Station (blue). Considering the sedimentation rate (0.2 cm/yr) in the study area, a 1 cm-thick sediment is deposited during the 5-year period. Monthly mean SST in (c) February 2012 and (d) August 2012, derived from NOAA satellite data. Images are provided by the National Fisheries Research and Development Institute (NFRDI), Korea. White rectangle indicates the study area. .... 8

**Fig. 3.** Spatial variations of the core-top alkenone temperature at (a)

present and (b) 6.5 kyr B.P. Colored circle indicates temperature (see index). Black lines (310, 311, and 312) and small dot in (a) indicate the oceanographic observation lines and station of the NFRDI. (c) 5-year (2010–2014) average *in situ* SST obtained at two-month intervals at the two landward observation stations. Dashed line indicates the average *in situ* SST in April to October at each of the NFRDI observation line. Yellow shading represents the present range of the core-top alkenone temperature. Gray shading indicates the monthly chlorophyll-a concentration in the HMB during 2012–2013 (datasets from the Korea Marine Environment Management Corporation, Korea). ..... 14

**Fig. 4.** Alkenone-based SST changes versus calendar age for cores HMB-103 and HMB-102. Inverted triangle indicates radiocarbon date and calendar age. Horizontal bar represents  $1\sigma$  error range of calendar age. .... 17

**Fig. 5.** Comparison of Holocene surface temperature records for East Asia. (a) The map shows the location of the HMB and other sites used for comparison in this study. (b) Alkenone-based SST changes in the southeastern Yellow Sea. (c) Pollen-based summer SAT changes at Lake Bayanchagan (Jiang et al., 2010). (d) Pollen-based annual SAT changes at Lake Chaohu in the lower Yangtze region (Li et al., 2018). (e) Alkenone-based summer SAT changes at Lake Qinghai, northeastern Tibetan Plateau (Hou et al., 2016). (f) Pollen-based annual SAT changes at Lake Ximencuo, eastern Tibetan Plateau (Herzschuh et al., 2014). (g)  $\delta^{18}\text{O}$  record from the Guliya ice core, western Tibetan Plateau (Thompson et al., 1997). (h) *G. ruber* Mg/Ca-based summer SST changes in the northern East China Sea (Kubota et al., 2010). (i) *G. ruber* Mg/Ca-based summer SST changes



in the middle Okinawa Trough (Sun et al., 2005). Dashed line represents the linear regression. Inverted triangle indicates radiocarbon dating. .... 19

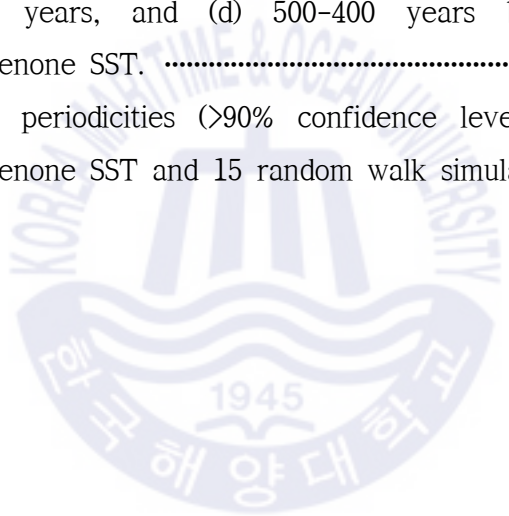
**Fig. 6.** (a) The locations of cores from high- and low-latitudes used in this study. (b) Alkenone-based SST changes in this study. (c) Planktonic foraminiferal MAT-based summer SST changes in the Barents Shelf (Sarnthein et al., 2003). (d) Alkenone-based annual SST changes in the western equatorial Atlantic (Ruhlemann et al., 1999), eastern equatorial Pacific (Kienast et al., 2006), and South China Sea (Zhao et al., 2006). (e) SST gradient between the high-latitude Barents Sea and low-latitude tropics. (f) ESR intensity of silt-sized quartz from core D-GC-6 in the East Sea (Nagashima et al., 2013). Inverted triangle indicates radiocarbon dating. .... 24

**Fig. 7.** (a) Alkenone-based SST changes in this study. (b) Reconstructed sea-level curves for western Pacific regional seas (Chough et al., 2004; Liu et al., 2004; Zong, 2004; Choi, 2009; Tjallingii et al., 2014). (c) Calculated Simpson-Hunter parameter [ $\log(H/u^3)$ ], which indicates the magnitude of coastal tidal mixing at the location of core HMB-102. (d) Abundance of *P. obliquiloculata* in the Okinawa Trough (Jian et al., 2000). Inverted triangle indicates radiocarbon dating. .... 27

**Fig. 8.** (a) High-resolution alkenone-based SST changes versus calendar age for core HMB-103. Inverted triangles indicate the radiocarbon dates. Gray shading indicates the error range of SST. Inverted triangle indicates radiocarbon dating. (b) Spectral analyses result for HMB-103 alkenone SST (raw data). .... 35

**Fig. 9.** (a) 2000–50 years band-pass filtered HMB-103 alkenone SST, and (b) the result of spectral analyses. Inverted triangle indicates

	radiocarbon dating. ....	36
<b>Fig. 10.</b>	Comparison of the HMB-103 SST with the tree ring growth index in Japan (Cook et al., 2013) over the last 2000 years. ....	38
<b>Fig. 11.</b>	Comparison of (a) total solar irradiance (TSI) (Steinhilber et al., 2009) with (b) HMB-103 alkenone SST over the last 6.5 kyr B.P. (c) Spectral analyses results for alkenone SST and TSI. ....	39
<b>Fig. 12.</b>	Continuous transform wavelet spectra for the HMB-103 alkenone SST and TSI, and cross-wavelet spectrum between them. ....	41
<b>Fig. 13.</b>	Spectral analyses results for (a) 100–50 years, (b) 200–100 years, (c) 300–200 years, and (d) 500–400 years band-pass filtered HMB-103 alkenone SST. ....	42
<b>Fig. 14.</b>	Significant periodicities (>90% confidence level) present in the HMB-103 alkenone SST and 15 random walk simulations. ....	44



# Holocene variability in sea surface temperature off the southwest coast of Korea and its implications for East Asia climate changes

Bae, Si Woong

Department of Convergence Study on the Ocean Science and Technology  
Ocean Science and Technology School  
Korea Maritime and Ocean University

## Abstract

To reconstruct the variations in sea surface temperature (SST) during the Holocene, the alkenone unsaturation index of marine sediments from two deep-drilled cores and 81 different core-top surface sediments recovered from the Heuksan Mud Belt, located off the southwestern coast of the Korean Peninsula, was measured. First, comparison of the alkenone temperature estimates of 81 core-top sediments with *in situ* temperatures indicates that the alkenone temperatures correspond to the average SST in April to October. The spatial distribution pattern of the core-top alkenone SST shows a north-south temperature gradient, which represents the *in situ* temperatures well. This indicates that the effects of the resuspension and lateral transport of sediments on the past temperature estimation might be insignificant. Based on the two deep-drilled cores, variations in the alkenone SST during the Holocene were reconstructed. In general, the alkenone SST decreased by less than 1°C from the early to late Holocene. An interesting feature is the presence of two long

and pronounced cold (approximately 2°C) periods, which occurred at 3–5 kyr and 6.6–8.4 kyr B.P. These cold periods were also observed in other mid-latitude regions in East Asia, indicating that the cooling pattern was regional. The cold periods appear to be associated with the southward migration of the westerly jet at that time. Investigations into the effects of local sea level changes and resultant changes in tidal regime on changes in the SST during the Holocene period suggest that they were insignificant in the study area.

Herein, we elucidate continuous variations of alkenone SST over the last 6.5 kyr B.P. at a high-resolution (10–20 year) by using records from marine sediments of deep-drilled core HMB-103, which are recovered from the Heuksan mud belt. The high-resolution SST record allows the detection of centennial-scale fluctuations with various cycles. The spectral and wavelet analysis of alkenone SST revealed significant periodicities of 415, 227, 145, 102, 83, and 73 years at >90% confidence level. These periods exhibit extreme proximity to the solar activity cyclicities of ~400, 210 (Suess/de Vries cycles), 150, and 120–60 years (Gleissberg cycles). This indicates a linkage between the variations of HMB-103 alkenone SST and solar activity at the centennial scale over the last 6.5 kyr B.P.

**KEY WORDS:** Alkenone; Sea surface temperature; Holocene; Yellow Sea; Palaeoclimatology; Centennial variance; Solar Activity

# 홀로세 한반도 서남해 연안 표층수온변화와 동아시아 기후변화

배시웅

한국해양대학교 해양과학기술전문대학원  
해양과학기술융합학과

## 요약

본 연구에서는 한반도 서남해 연안에 위치한 흑산머드벨트에서 채취된 2개의 심부시추코어 (HMB-102, HMB-103) 퇴적물과 같은 곳에서 별도로 채취된 81개 표층퇴적물의 알케논 분석을 통해 홀로세동안 표층수온변화를 복원하였다. 먼저 81개 표층퇴적물의 알케논수온과 관측수온을 비교하여 연구지역에서 해양퇴적물로부터 복원한 알케논수온은 4-10월 평균 표층수온을 대표함을 확인하였다. 특히 표층퇴적물 알케논 수온분포는 북쪽은 낮고, 남쪽은 높은 관측수온 분포와 유사하다. 이는 퇴적물의 재부유나 수평이동이 과거 표층수온 복원에 주는 영향은 작다는 것을 의미한다. 심부시추코어 퇴적물 알케논 분석을 통해 지난 홀로세동안 표층수온변화를 복원하였다. 초기 홀로세부터 현재까지 알케논수온은 전반적으로 1°C정도 감소한다. 그리고 특징적으로 3-5 kyr B.P.와 6.6-8.4 kyr B.P. 사이에 2°C정도의 강하고 지속적인 한랭기간이 존재함을 발견하였다. 이 기간은 동아시아 다른 지역 (티벳고원, 중국 북동부, 양쯔강 유역, 오키나와트러프)에서도 발견되며 동아시아 중위도 지역의 지역적인 특징임을 확인하였다. 동아시아 중위도 지역에서 전반적으로 관찰되는 홀로세동안 두 번의 장기간 한랭기는 당시 Westerly Jet 경로가 상대적으로 남쪽으로 이동한 것과 연관된 것으로 생각

된다. 반면 홀로세 해수면 변동과 그와 관련된 조석변화를 고려하면 이들은 흑산머드벨트 표층수온 변화에 큰 영향을 주지는 못한 것 같다.

HMB-103 시추코어퇴적물의 추가적인 알케논 분석을 통해 지난 6.5 kyr B.P. 동안 표층수온 변화를 고해상도로 (10-20년 변화) 복원하였다. 이때 연구지역에서 수백 년 규모의 수온변동이 존재함을 확인하였다. 알케논 수온자료의 spectral과 wavelet 분석결과 90%이상의 신뢰구간에서 415, 227, 145, 102, 83, 73년의 주기가 뚜렷하다. 알케논 수온변화에서 발견된 주기들은 홀로세동안 태양활동변화 주기인 ~400, 210 (Suess/de Vries cycles), 150, and 120-60 years (Gleissberg cycles)와 유사하다. 이는 지난 6.5 kyr B.P.동안 태양활동변화와 HMB-103 알케논 수온의 수백 년 주기변동 사이에 관련이 있음을 의미한다.

**KEY WORDS:** 알케논; 표층수온; 홀로세; 황해; 고기후; 수백 년 규모 변동성; 태양활동

---

※ 학위논문 제 2장에 개제된 상당수의 내용과 그림은 이미 국제전문학술지인 Palaeogeography, Palaeoclimatology, Palaeoecology에 온라인 출판되어 발표되었음.

Bae, S.W., Lee, K.E., Chang, T.S., 2019. The long and pronounced cold periods 3,000-5,000 and 6,600-8,400 years B.P. in East Asia and the southward migration of the westerly jet. Palaeogeography, Palaeoclimatology, Palaeoecology, doi:<https://doi.org/10.1016/j.palaeo.2019.109402>

## Chapter 1. Introduction

The reconstruction of the paleoclimate is important to understand the natural variation and evolution of the current climate because instrumental records only span a tiny part (~100 years) of Earth's history. In particular, the reconstruction of historical sea surface temperature (SST) is important as it aids the understanding of ocean behavior during climate change; it allows us to validate numerical climate models and assess the significance of current climate trends. Recently, numerous researchers have attempted to reconstruct spatio-temporal changes in historical SSTs and synthesize them. Global SST reconstructions for the Last Glacial Maximum and the Holocene were published by the Multiproxy Approach for the Reconstruction of the Glacial Ocean Surface (MARGO) project (MARGO Project Members, 2009) and the Global Holocene Spatial and Temporal Climate Variability (GHOST) project (Leduc et al., 2010), respectively.

The Holocene corresponds to the last 11,700 years of the Earth's history. This period represents the present interglacial after the last deglaciation followed by the Last Glacial Maximum. The Holocene was known to have a relatively warm and stable climate compared to the last glacial and deglaciation periods. However, with the accumulation of more paleoclimate records, it seems that the Holocene climate was not as stable as previously thought. Millennial- to centennial-scale paleoclimatic variations during the Holocene have been reported in various parts of the world (Bond et al., 2001; Wang et al., 2005; Marchitto et al., 2010; Masson-Delmotte et al., 2013; Bakker et al., 2017). The cause of climate variation at millennial to centennial time scales during the Holocene remains under debate; this is particularly due

to the lack of high-resolution and continuous paleoclimate records.

Chapter 2 describes the carefully reconstructed SST records during the Holocene using the alkenone unsaturation index of marine sediments of two deep-drilled cores (HMB-102 and HMB-103) and 81 different core-top sediments that were recovered from the southwest coast of Korea. First, we compared the alkenone SSTs of 81 core-top sediments with in situ SSTs to test the applicability of alkenone paleothermometry in the study area. Second, we reconstructed the Holocene SST record from deep-drilled sediments. We found that there were two long and pronounced cold periods at 3-5 and 6.6-8.4 years B.P. Finally, we examined several factors affecting SST changes.

Chapter 3 discusses the further alkenone analyses of HMB-103 sediments that were carried out to reconstruct a high-resolution SST record over the last 6.5 kyr B.P. The records have an average temporal resolution of approximately 10-20 years. Hence, centennial to millennial time scale SST variations can be investigated based on the alkenone record. The spectral and wavelet analyses of alkenone SST revealed significant (>90% confidence level) periodicities at the centennial time scale. We investigated the relationship between centennial-scale SST changes with solar activity.



## Chapter 2.

# Two long and pronounced cold periods 3,000–5,000 and 6,600–8,400 years B.P. in East Asia and the southward migration of the westerly jet

### 2.1 Introduction

Spatial and temporal reconstructions of surface temperature changes during the Holocene (i.e., the last 11,700 years) help us to understand natural climate variability and forcing mechanisms. According to a study on the synthesis of 73 globally distributed terrestrial and oceanic temperature proxy records (Marcott et al., 2013), the temperature during the early-middle Holocene was high and was followed by 0.7°C cooling in the late Holocene. However, variations in regional temperatures during the Holocene were not always consistent with those of the stacked temperature and variations occurred even at similar latitudes (Kim et al., 2004; Leduc et al., 2010; Clegg et al., 2011; Marcott et al., 2013; Harada et al., 2014; Marsicek et al., 2018).

The Holocene temperature records of East Asia have rarely been included in global temperature reconstruction studies (Wanner et al., 2011, 2015; Marcott et al., 2013; Masson-Delmott et al., 2013) because of limitations in data availability. Recently, the Holocene temperature variations in this region have been quantitatively reconstructed based on various proxies, including pollen, alkenone, and branched glycerol dialkyl glycerol tetraethers (brGDGT) from peat and lake sediments (Herzschuh et al., 2014; Hou et al., 2016; Li et

al., 2018; Zhang and Feng, 2018; Zhang et al., 2018; Zheng et al., 2018). However, most temperature variations have been reconstructed in high-altitude areas (e.g., Tibetan Plateau, Altai Mountains) with low temporal resolution. To accurately determine the climate change in East Asia, it is necessary to reconstruct a high-resolution and continuous temporal sea surface temperature (SST) record for the Holocene using marine sediment. Furthermore, compilation of regional temperature records, including SST, and comparison with high- and low- latitude temperature records is necessary to identify the characteristics of the surface temperature changes in East Asia and the associated forcing mechanism.

The Yellow Sea is a semi-enclosed marginal sea surrounded by Korea and China (mean water depth: 44 m; Fig. 1a). The Yellow Sea has undergone dramatic environmental changes due to global eustatic sea level changes during the late Quaternary period. During the last glacial maximum, when sea levels were ~120 m lower than today, the Yellow Sea shelf was subaerially exposed (Yoo et al., 2016). Subsequently, the sea level rose rapidly during the deglacial period, and it reached to present position at early Holocene (Qin et al., 1996; Liu et al., 2004). During the Holocene, thick mud deposits developed in certain areas of the Yellow Sea (Fig. 1a). These mud deposits are characterized by high sedimentation rates, allowing high-resolution studies of paleoenvironmental changes. The changes in SST in the area can be influenced by various factors, including changes in solar radiation (Lee et al., 2007), tidal mixing (Lie, 1989), the monsoon system, and the connection between atmosphere and ocean circulation and climate modes (Yeh and Kim, 2010; Kim et al., 2018).

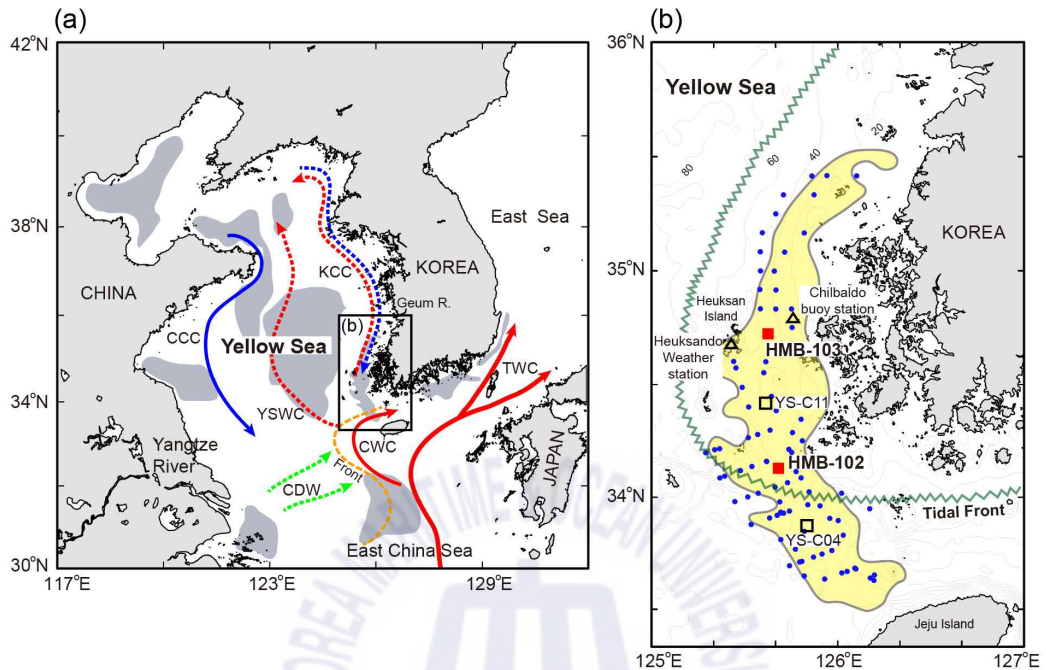


**Fig. 1.** (a) Distribution of Holocene mud deposits (dark gray shading) and surface currents in the Yellow Sea and East China Sea. Blue (red) arrow represents cold (warm) current. Dashed arrow indicates seasonally varying current. Orange dashed line represents the thermohaline front. TWC, Tsushima Warm Current; CWC, Cheju Warm Current; YSWC, Yellow Sea Warm Current; KCC, Korean Coastal Current; CCC, Chinese Coastal Current; CDW, Changjiang Diluted Water. (b) Bathymetric map of the study area (contours in m) and core locations. The Heuksan Mud Belt (HMB) is marked by yellow shading. Red and black square indicates the location of the two deep-drilled cores (HMB-102, HMB-103) and piston cores (YS-C11, YS-C04) (Park et al., 2000), respectively. Blue dot indicates the location of the core-top sediment. Black triangle indicates the Heuksando Weather Station and Chilbaldo Buoy Station of the Korea Meteorological Administration. Green zigzag line represents the distribution of the tidal front.

In this study, alkenone temperatures, estimated using 81 core-top sediments from the Heuksan Mud Belt (HMB) in the southeastern Yellow Sea, were compared with *in situ* temperatures to test the applicability of alkenone paleothermometry in the study area. In addition, we reconstructed variations in the SST during the Holocene by using the alkenone unsaturation index of marine sediments of two deep-drilled cores (HMB-102 and HMB-103) recovered from the HMB. We identified the characteristics of the HMB SST record during the Holocene and examined several factors affecting SST changes.

## 2.2 Geological and oceanographic settings

The HMB developed in a north-south direction along the southwestern coast of Korea (Fig. 1b). Water depths in the HMB range from 20 m in the north to 110 m in the south (Fig. 1b). In previous studies, the stratigraphy and evolution of the HMB during the Holocene has been investigated using seismic profiles and sediment cores (Lee et al., 2015; Chang and Ha, 2015). Based on  $^{210}\text{Pb}$  (Park et al., 2000) and  $^{14}\text{C}$  (Chang and Ha, 2015) dating (Table 1), it has been demonstrated that surface sediments collected above the latitude of  $34^\circ\text{N}$  are modern-day sediments, whereas those collected below  $34^\circ\text{N}$  are sediments from 6–7 kyr B.P.

Since the study area is located in relatively shallow water, changes in the SST are closely related to changes in air temperature and solar radiation. Comparison of the monthly mean *in situ* SST recorded at the Chilbaldo Buoy Station for the period of 1998–2018 (dataset from the Korea Meteorological Administration, KMA) with the concurrent *in situ* surface air temperature (SAT) obtained at the Heuksando Weather Station (dataset from the KMA) revealed similar temperature changes (Figs. 1b and 2a;  $r^2=0.89$ ,  $P<0.0001$ ,

n=235). The SST decreases to 5°C in winter due to cold and dry northwesterly winds and weak solar radiation, whereas it increases to 25°C in summer due to warm and wet southeasterly wind and strong solar radiation.

Oceanic fronts develop around the HMB throughout the year. In winter, a thermohaline front is established between the Cheju Warm Current (CWC), which rounds Jeju Island clockwise, and the Korean Coastal Current (KCC), which flows southward along the west coast of Korea (Fig. 1a; Lie and Cho, 2016). The Yellow Sea Warm Current (YSWC) intermittently penetrates into the Yellow Sea across the front (Lie et al., 2001; Lie and Cho, 2016). In summer, the CWC retreats to the west coast of Jeju Island due to the intrusion of Changjiang Diluted Water (CDW); the thermohaline front also weakens. A strong tidal front is established in summer between well-mixed coastal regions and stratified open ocean regions (Fig. 1b; Lie, 1989).

The Yellow Sea is strongly affected by semidiurnal tides. The tidal range in the HMB exceeds 3 m and the maximum current velocity ranges between 80 and 100 cm/s (Lee and Chu, 2001; Chang et al., 2015). The summer SST in the well-mixed coastal region is lower than in the stratified regions due to vertical mixing by tidal stirring (Lie, 1989). However, if 5-year average temperatures, which correspond to an approximately 1 cm-thick sediment layer in the study area, are calculated using the monthly temperatures (Fig. 2b), the effect of tidal mixing on the SST decrease is smoothed and becomes insignificant.

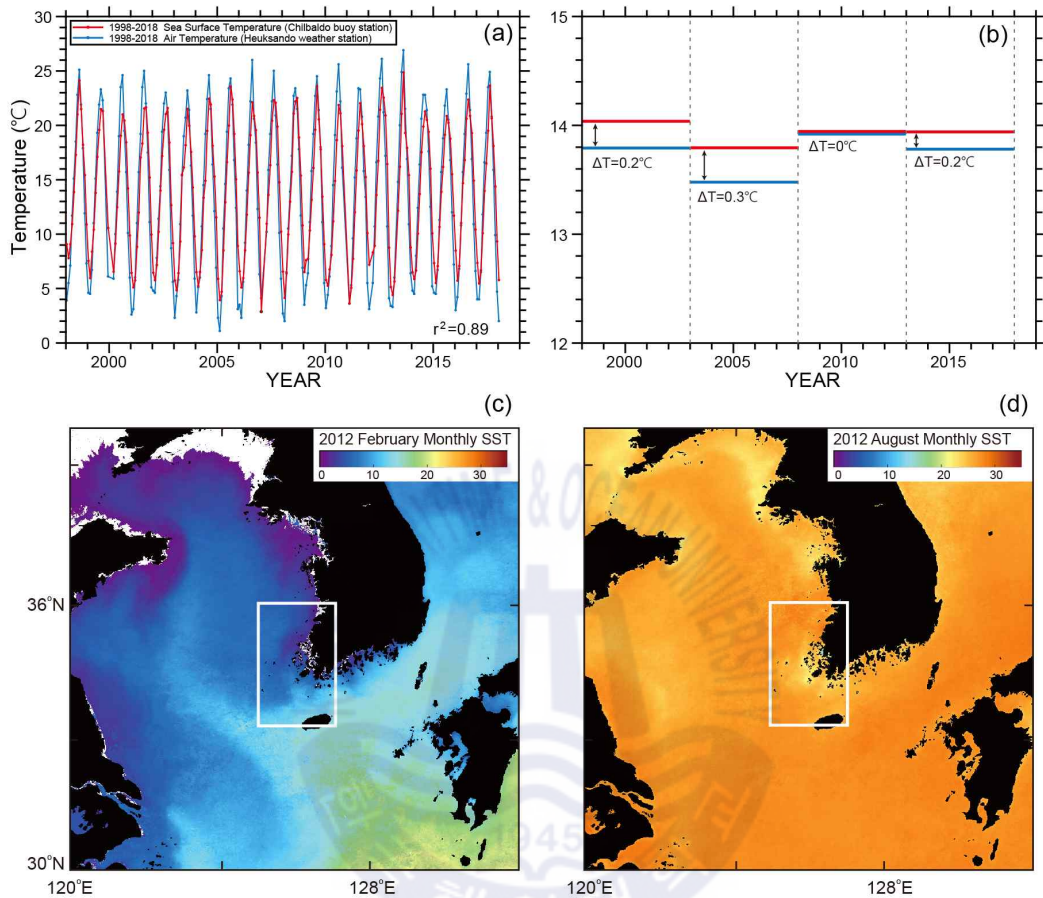


**Fig. 2.** (a) Monthly fluctuation (1998 and 2018) and (b) 5-year average values of the SST at the Chilbaldo Buoy Station (red) and SAT at the Heuksando Weather Station (blue). Considering the sedimentation rate (0.2 cm/yr) in the study area, a 1 cm-thick sediment is deposited during the 5-year period. Monthly mean SST in (c) February 2012 and (d) August 2012, derived from NOAA satellite data. Images are provided by the National Fisheries Research and Development Institute (NFRDI), Korea. White rectangle indicates the study area.

## 2.3 Materials and methods

In this study, marine sediments from two deep-drilled cores, HMB-102 (34° 7.96'N, 125° 40.94'E, water depth: 57 m) and HMB-103 (34° 43.50'N, 125° 37.51'E, water depth: 48 m), were used. They were obtained by the Korean Institute of Geoscience and Mineral Resources (KIGAM) in 2013 using the Chinese drill ship KAN 407 (Fig. 1b). These cores mainly consisted of gray mud with silt streaks and wave-formed ripples (Chang and Ha, 2015). Only Holocene muddy sediments from the upper 21 meters below sea floor (mbsf) in HMB-102 and upper 13 mbsf in HMB-103 were used for alkenone analyses. The 1 cm-thick samples were collected at approximately 10–30 cm intervals for HMB-102 and at 15 cm intervals for HMB-103. In addition, 81 core-top sediments (0–1 cm) were used for the alkenone analyses. They were subsampled from box, piston, and vibro cores obtained by the KIGAM during HMB cruises in 2012–2014 (Fig. 1b).

The ages of the two deep-drilled cores, HMB-102 and HMB-103, were determined by radiocarbon dating in a previous study (Table 1; Chang and Ha, 2015). The accelerator mass spectrometry (AMS)  $^{14}\text{C}$  ages of benthic foraminifera and bivalve shells were measured at the Institute of Geological Nuclear Science, New Zealand and KIGAM, Korea, respectively. The AMS  $^{14}\text{C}$  ages were converted to calendar ages using CALIB 7.1 (Stuiver et al., 2015). The marine reservoir correction ( $\Delta R$ ) was used as the zero value due to uncertainty in the study area. The results of  $^{210}\text{Pb}$  dating of the HMB marine sediments were presented in the previous study (Table 1; Park et al., 2000). They observed excess  $^{210}\text{Pb}$  activities at core YS-C11 collected above the latitude of 34° N, indicating that the core-top surface sediments are modern-day sediments. In contrast, the absence of excess  $^{210}\text{Pb}$  activities in core YS-C04 collected below 34° N suggests that the core-top surface

**Table 1.**  $^{14}\text{C}$  ages for core HMB-103 and HMB-102 and  $^{210}\text{Pb}$  ages for core YS-C11 and YS-C04

Core ID	Sample Depth (cm)	Material	AMS $^{14}\text{C}$ age (yr B.P.)	Total $^{210}\text{Pb}$ (dpm/g)	$^{226}\text{Ra}$ (dpm/g)	Excess $^{210}\text{Pb}$ (dpm/g)	Calendar Age (yr B.P.)	Calendar Age (yr before 1997)	Ref
HMB-103	300	Shell	1,570±40	-	-	-	1,123±55	-	(1)
	500	Bulk benthic foram.	2,761±21	-	-	-	2,473±70	-	(1)
	720	Bulk benthic foram.	3,581±22	-	-	-	3,476±42	-	(1)
	1,140	Bulk benthic foram.	5,435±24	-	-	-	5,815±48	-	(1)
HMB-102	500	Bulk benthic foram.	6,201±25	-	-	-	6,648±41	-	(1)
	610	Bulk benthic foram.	6,922±27	-	-	-	7,434±27	-	(1)
	650	Bulk benthic foram.	7,890±60	-	-	-	8,354±59	-	(1)
	800	Shell	8,484±30	-	-	-	9,078±60	-	(1)
	1,100	Bulk benthic foram.	8,935±30	-	-	-	9,570±44	-	(1)
	1,280	Bulk benthic foram.	8,995±31	-	-	-	9,636±65	-	(1)
YS-C11	0	Dry sediment	-	4.2	1.5	2.7	-	0	(2)
	3	Dry sediment	-	3.1	1	2.1	-	8	(2)
	10	Dry sediment	-	2.1	1.1	1	-	26	(2)
	14	Dry sediment	-	2	1.1	0.9	-	36	(2)
YS-C04	0	Dry sediment	-	1.4	-	-	-	-	(2)
	10	Dry sediment	-	1.3	-	-	-	-	(2)
	20	Dry sediment	-	1.2	-	-	-	-	(2)
	25	Dry sediment	-	1.5	1.4	-	-	-	(2)
	30	Dry sediment	-	1.5	-	-	-	-	(2)
	35	Dry sediment	-	1.2	1.1	-	-	-	(2)

(1) indicates Chang and Ha (2015).

(2) indicates Park et al. (2000).



sediments in the southern part are old sediments. The old sediment could be 6.5 kyr B.P. according to  $^{14}\text{C}$  dating (Chang and Ha, 2015). The calendar age of HMB-103 is 1.1 kyr B.P. at 3 mbsf and 5.8 kyr B.P. at 11.4 mbsf. For HMB-102, the interval of 5–12.8 mbsf contains records dating from 6.6–9.6 kyr B.P. Therefore, these two deep-drilled sediment cores allowed us to reconstruct SST changes during the entire Holocene.

We analyzed  $\text{C}_{37}$  alkenone by using freeze-dried sediments (2 g) for SST reconstruction. The  $\text{C}_{37}$  alkenones were measured at the Korea Maritime and Ocean University. The sediments were extracted using an accelerated solvent extractor (ASE-200, Dionex Corporation) with the solvent ( $\text{CH}_2\text{Cl}_2\text{:MeOH}$ , 99:1) maintained at  $100^\circ\text{C}$  and 1500 psi for 10 min. The extracted organic matter was cleaned by elution with  $\text{CH}_2\text{Cl}_2$  ( $500 \mu\text{L} \times 3$ ) through a silica cartridge (Silica SPE cartridge, 100 mg/ml, Agilent Technologies). Subsequently, 0.1 M hydroxide potassium (KOH) was added to the samples for saponification. The samples were maintained at  $70^\circ\text{C}$  for 2 h to allow the chemical reaction to occur. The alkenone fraction was obtained by partitioning into hexane. After being concentrated under  $\text{N}_2$ , the alkenones were separated from the final extract using a gas chromatograph (Shimadzu 17-A) equipped with a flame ionization detector and fused-silica capillary column (J&W DB-1,  $0.32 \text{ mm} \times 0.25 \mu\text{m} \times 60 \text{ m}$ , Agilent Technologies). The degree of unsaturation ( $U_{37}^{k'}$ ) was calculated using Eq. (1) (Prahl and Wakeham, 1987) and the alkenone temperature was reconstructed using Eq. (2) (Prahl et al., 1988).

$$U_{37}^{k'} = [\text{C}_{37:2}] / ([\text{C}_{37:2}] + [\text{C}_{37:3}]) \quad (1)$$

$$U_{37}^{k'} = 0.034T + 0.039 \quad (2)$$

The reproducibility of the alkenone temperature assessment for replicate samples (n=84) of a homogeneous marine sediment laboratory standard exhibits differences of less than  $\pm 0.3^{\circ}\text{C}$  at the 95% confidence level.

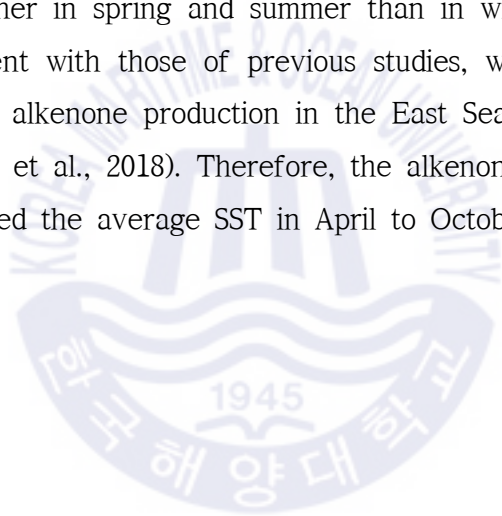
## 2.4 Results

### 2.4.1 Core-top sediments

The spatial distribution patterns of the alkenone temperatures, estimated using 81 core-top sediments, are illustrated in Figure 3a and b. The results of  $^{210}\text{Pb}$  dating (Park et al., 2000) indicates that core-top sediments located above the latitude of  $34^{\circ}\text{N}$  were present-day sediments (Fig. 3a), whilst  $^{14}\text{C}$  dating (Chang and Ha, 2015) indicates that the age of the sediments located below this latitude (Fig. 3b) were 6.5 kyr B.P. For the present-day sediments shown in Figure 3a, the alkenone temperatures in the northern part of Heuksan Island ( $34^{\circ}40'\text{N}$ ) were relatively low, ranging between  $16^{\circ}\text{C}$  and  $17.5^{\circ}\text{C}$ . However, those in the southern part were generally high, ranging between  $17.5^{\circ}\text{C}$  and  $18.5^{\circ}\text{C}$  (Fig. 3a). For the core-top sediments shown in Figure 3b, collected below  $34^{\circ}\text{N}$ , the alkenone temperatures were  $18^{\circ}\text{C}$ - $22^{\circ}\text{C}$  and the temperatures markedly increased toward the southern limit of the HMB. This pattern was consistent with that of the *in situ* SST derived from National Oceanic and Atmospheric Administration (NOAA) satellite data (Fig. 2c and d). Hence, the alkenone temperatures derived from both the present-day and 6.5 kyr B.P. sediments showed a north-south temperature gradient, which resembled the *in situ* SST pattern, indicating that the effects of the resuspension of sediments and lateral transport of suspended materials on the past temperature estimation might be insignificant in the study area.

To determine the season of alkenone production in the study area, the

alkenone temperatures of present-day sediments (Fig. 3a) were compared with *in situ* temperatures obtained by the National Fisheries Research and Development Institute (NFRDI), Korea (Fig. 3c). These are 5-year (2010–2014) average *in situ* SST data obtained at two-month intervals from two landward stations at each of the 310, 311, and 312 NFRDI observation lines (Fig. 3a). The alkenone temperatures and their spatial distribution patterns corresponded well with those of the average *in situ* SST in April to October. In addition, the monthly mean concentrations of chlorophyll-a at the HMB, obtained by the Korea Marine Environment Management Corporation (KOEM) during 2012–2013, were higher in spring and summer than in winter (Fig. 3c). These results were consistent with those of previous studies, which investigated the season and depth of alkenone production in the East Sea and East China Sea (Lee et al., 2014; Ko et al., 2018). Therefore, the alkenone temperature in the study area represented the average SST in April to October.



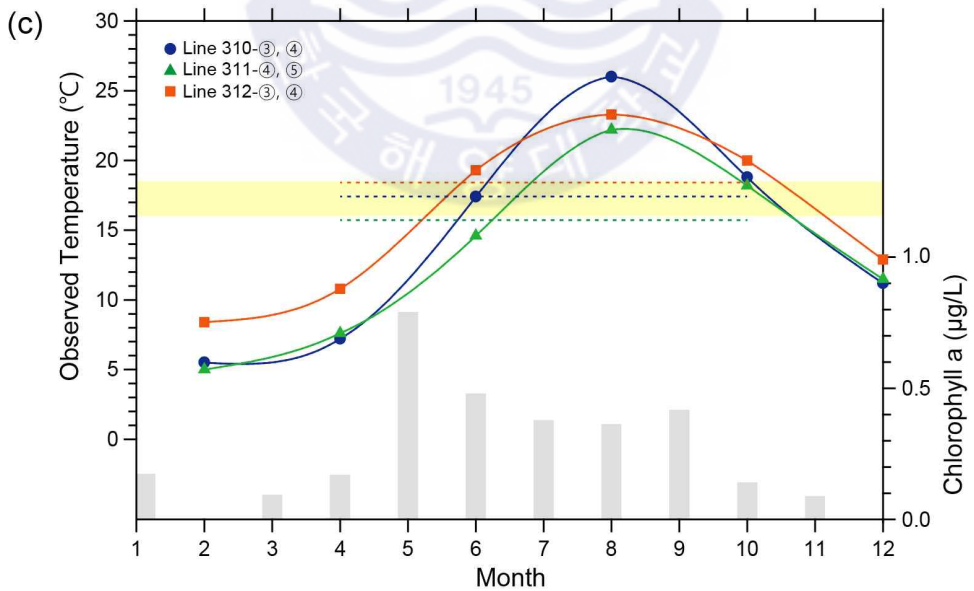
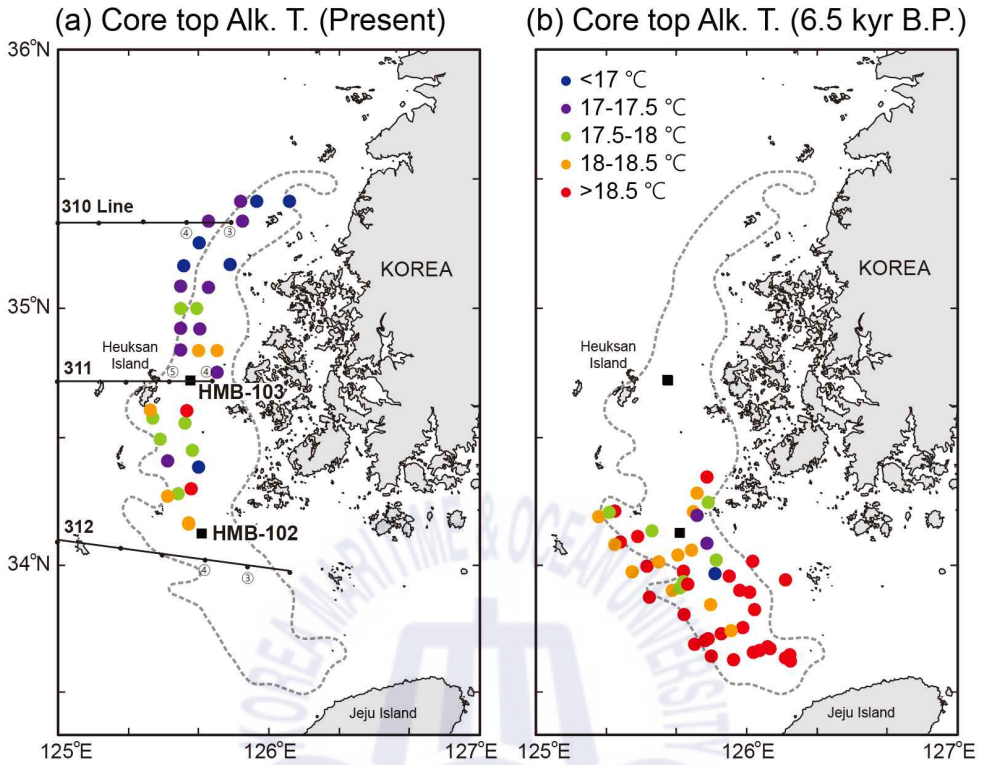


**Fig. 3.** Spatial variations of the core-top alkenone temperature at (a) present and (b) 6.5 kyr B.P. Colored circle indicates temperature (see index). Black lines (310, 311, and 312) and small dot in (a) indicate the oceanographic observation lines and station of the NFRDI. (c) 5-year (2010–2014) average *in situ* SST obtained at two-month intervals at the two landward observation stations. Dashed line indicates the average *in situ* SST in April to October at each of the NFRDI observation line. Yellow shading represents the present range of the core-top alkenone temperature. Gray shading indicates the monthly chlorophyll-a concentration in the HMB during 2012–2013 (datasets from the Korea Marine Environment Management Corporation, Korea).



#### 2.4.2 Deep-drilled core sediments

Variations in the SST of the southeast Yellow Sea during the Holocene, reconstructed from two deep-drilled cores, are illustrated in Figure 4. The long-term change in the alkenone temperature exhibited a decrease of 1°C during the entire Holocene (Fig. 5b). In HMB-102, the alkenone temperature from 8.4–9.6 kyr B.P. was relatively warm, with an average temperature of 19°C. It then decreased by more than 1°C until 6.6 kyr B.P.; the average temperature from 6.6–8.4 kyr B.P. was 17.5°C. In HMB-103, the average alkenone temperatures for the periods 5–6.5 and 0–3 kyr B.P. was 18°C. From 3–5 kyr B.P., the temperature dropped by 2°C and the average temperature was 16.5°C. Thus, two long and pronounced cold periods occurred at 3–5 and 6.6–8.4 kyr B.P., although in general, the Holocene was characterized by a relatively stable climate compared to the glacial–interglacial changes. Considering that globally averaged surface temperature data shows a warming of 0.85°C during the period 1880–2012 (Masson-Delmott et al., 2013), the two cold periods during the Holocene were distinct and the magnitude of cooling was large.

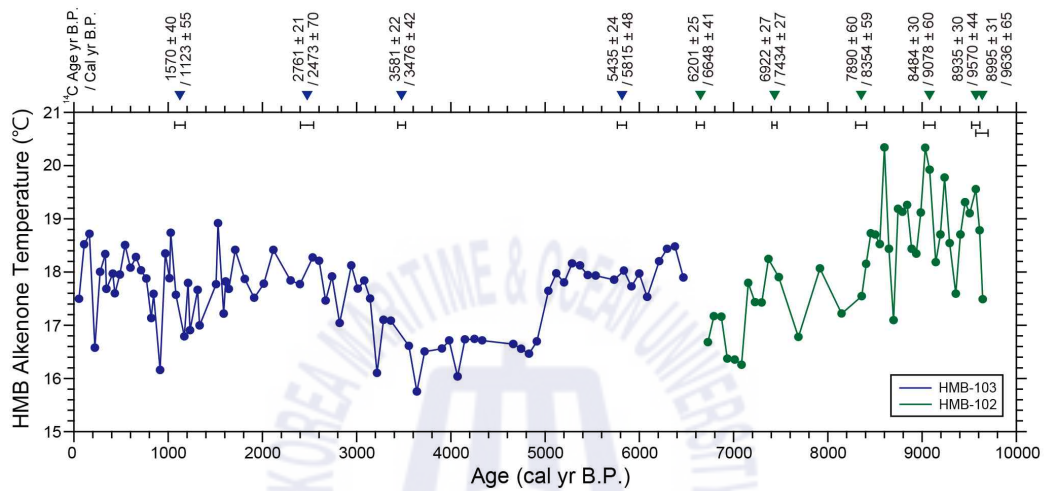


**Fig. 4.** Alkenone-based SST changes versus calendar age for cores HMB-103 and HMB-102. Inverted triangle indicates radiocarbon date and calendar age. Horizontal bar represents  $1\sigma$  error range of calendar age.

## 2.5 Discussion

### 2.5.1 Regional surface temperature changes

To investigate whether the two long and pronounced cold periods from 3–5 and 6.6–8.4 kyr B.P. were local characteristics of the Yellow Sea or regional patterns in East Asia, the HMB SST record was compared with Holocene surface temperature records from the mid-latitudes of East Asia (Fig. 5). Seven previously published surface temperature records were chosen because: (1) they provide quantitative temperature records; (2) the seasonality of the records has been well documented; and (3) the stratigraphy and age dating of the cores are reasonable. For pollen-based temperature records, statistically meaningful data were collected by counting at least 300 pollen grains in each sample (Fig. 5c, d, f). Recent attempts have been made to reconstruct the quantitative Holocene SAT using brGDGT in Chinese peat and lake sediments (Li et al., 2017; Zheng et al., 2018). However, these records were not included because the pattern of the reconstructed SAT could vary depending on the calibration equations used.

The locations at which the East Asia surface temperature records were reconstructed are illustrated in Figure 5a. The pollen-based summer SAT record was reconstructed from Lake Bayanchagan, Northeast China (Fig. 5c; Jiang et al., 2010). The pollen-based annual mean SAT record was reconstructed from Lake Chaohu in the lower Yangtze region (Fig. 5d; Chen et al., 2009; Li et al., 2018). The alkenone-based summer temperature record was reconstructed from Lake Qinghai in the northeastern Tibetan Plateau (Fig. 5e; Hou et al., 2016). The pollen-based annual mean SAT record was reconstructed from Lake Ximencuo in the eastern Tibetan Plateau (Fig. 5f; Herzschuh et al., 2014). The  $\delta^{18}\text{O}$  record from the Guliya ice core from the



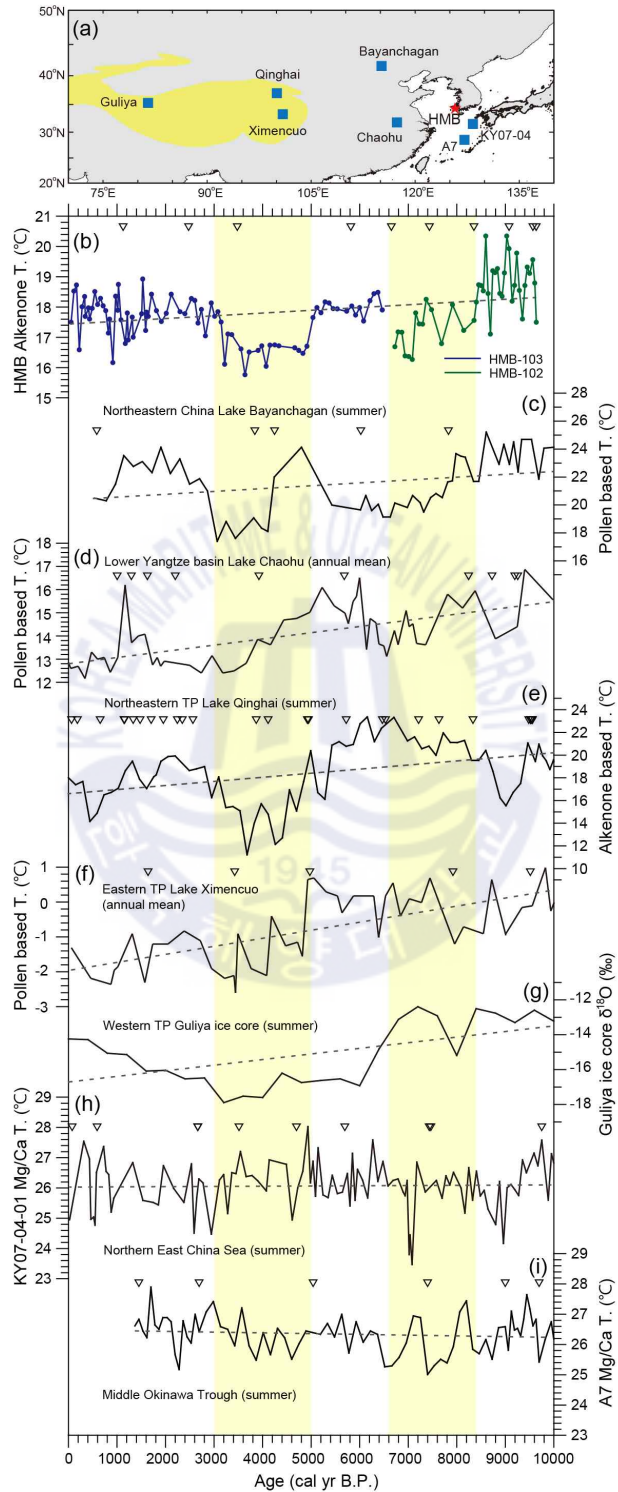
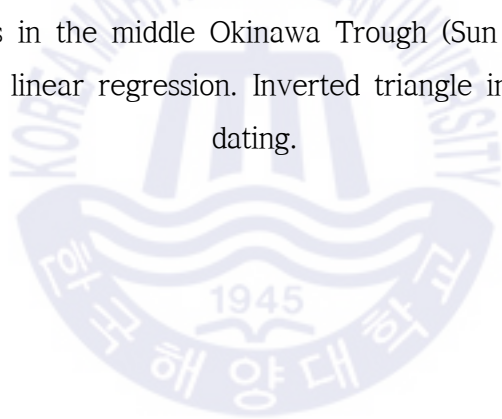


**Fig. 5.** Comparison of Holocene surface temperature records for East Asia. (a) The map shows the location of the HMB and other sites used for comparison in this study. (b) Alkenone-based SST changes in the southeastern Yellow Sea. (c) Pollen-based summer SAT changes at Lake Bayanchagan (Jiang et al., 2010). (d) Pollen-based annual SAT changes at Lake Chaohu in the lower Yangtze region (Li et al., 2018). (e) Alkenone-based summer SAT changes at Lake Qinghai, northeastern Tibetan Plateau (Hou et al., 2016). (f) Pollen-based annual SAT changes at Lake Ximencuo, eastern Tibetan Plateau (Herzschuh et al., 2014). (g)  $\delta^{18}\text{O}$  record from the Guliya ice core, western Tibetan Plateau (Thompson et al., 1997). (h) *G. ruber* Mg/Ca-based summer SST changes in the northern East China Sea (Kubota et al., 2010). (i) *G. ruber* Mg/Ca-based summer SST changes in the middle Okinawa Trough (Sun et al., 2005). Dashed line represents the linear regression. Inverted triangle indicates radiocarbon dating.



western Tibetan Plateau was used as a proxy for the past summer SAT (Fig. 5g; Yao et al., 1996; Thompson et al., 1997). For the SST records, *Globigerinoides ruber* Mg/Ca-based summer SST records, reconstructed from the northern East China Sea (Fig. 5h; Kubota et al., 2010) and middle Okinawa Trough (Fig. 5i; Sun et al., 2005), were used. Although the resolution of these surface temperature records from mid-latitudes in East Asia is lower than that recorded in this study, they show that variations in the surface temperatures at other sites in East Asia exhibit fluctuations on a multi-millennial timescale during the Holocene, similar to those observed in the HMB.

The cold period of 6.6–8.4 kyr B.P. observed in the HMB SST record could be identified in the summer and annual SAT records from the eastern part of China (Fig. 5c and d). A similar cooling was observed in the Mg/Ca summer SST records from the East China Sea and Okinawa Trough (Fig. 5h and i). In contrast, both the summer and annual SATs in the Tibetan Plateau above an altitude of 3000 m remained warm throughout the same period (Fig. 5e–g). During the period 3–5 kyr B.P., the surface temperatures were consistently low throughout East Asia, except for the northern region of the East China Sea. These results indicated that the two long and pronounced cold periods during the Holocene were regional patterns in the mid-latitudes of East Asia, although the cooling from 6.6–8.4 kyr B.P. was confined to the eastern part of Asia.

In the eastern part of Asia, the vegetation of the lower Yangtze region, Lake Chaohu, consists of a “subtropical evergreen–deciduous mixed broadleaved forests” at the present (Li et al., 2018). During the cold periods at 6.6–8.4 and 3–5 kyr B.P., conifers (e.g. *Pinus*) were dominant in East Asia, whereas the percentage of broadleaved evergreen trees (e.g. *Quercus-Cyclobalanopsis*) decreased. This vegetation change corresponded to

surface temperature changes in this area. On the other hand, in the western part of Asia near Lake Ximencuo (elevation, 4000 m), during the early Holocene, *Picea/Pinus* forest dominated until 5 kyr B.P. (Herzschuh et al., 2014). Then, the composition of vegetation changed from *Picea/Pinus* forest to mixture of alpine meadows and shrublands after 5 kyr B.P. This vegetation change is also consistent with temperature change at the highland area.

A long-term decline in the surface temperature in East Asia was apparent throughout the entire Holocene (Fig. 5). The magnitude of the long-term cooling of the terrestrial temperature ( $-2.6^{\circ}\text{C}/10$  kyr on average) was larger than that of the HMB SST record ( $-1^{\circ}\text{C}/10$  kyr). The overall cooling pattern was consistent with that of the Northern Hemisphere mid- to high-latitude Holocene temperatures, which is characterized by a warm early Holocene and gradual cooling in the middle-late Holocene (Marcott et al., 2013). The high-latitude Barents Sea summer SST record also shows an overall cooling trend during the Holocene (Fig. 6c; Sarnthein et al., 2003). These patterns correspond with a declining Northern Hemisphere summer insolation of  $\sim 40$   $\text{W}/\text{m}^2$  during the Holocene. In contrast, the annual mean SST records from low-latitudes show a gradual warming trend (Fig. 6d; Ruhlemann et al., 1999; Kienast et al., 2006; Zhao et al., 2006). This coincides with the increase in the annual mean insolation in the tropics during the Holocene. However, the two cold periods at 3–5 and 6.6–8.4 kyr B.P., simultaneously observed in the East Asia and Barents Sea, could not solely be explained by the gradually decreasing summer insolation during the Holocene but might be related to changes in regional atmospheric and oceanic conditions.

### 2.5.2 Potential factors affecting the SST changes

The mid-latitudes of East Asia are located on the migration route of the westerly jet (WJ), which seasonally moves in a north-south direction. At

present, the main route of the WJ lies in the south of the Himalayas ( $<30^\circ$  N) during winter and moves to the north of the Tibetan Plateau ( $>42^\circ$  N) during summer (Schiemann et al., 2009; Chiang et al., 2015). It has been suggested that the strength and position of the WJ are related to changes in the temperature gradient between the equator and poles (e.g., Holton, 2004; Kong et al., 2017; Zhang et al., 2018). An increased temperature gradient leads to a strengthened WJ and southward shift in its location. The variations in the WJ position during the Holocene were previously reported (Nagashima et al., 2013). Figure 6f shows the changes in the electron spin resonance (ESR) intensity of silt-sized quartz in marine sediments from the East Sea (Nagashima et al., 2013). A large ESR value indicates increased dust input from the Mongolian Gobi Desert, suggesting the southward displacement of the WJ position. Although no ESR data are available for the period from 6.6 to 8.4 kyr B.P., a clear increase in the ESR intensity can be observed between 3 and 5 kyr B.P. Calculations of the SST gradients between the high-latitude Barents Sea (Fig. 6c) and low-latitude tropics (Fig. 6d) demonstrated that the gradients at 3–5 kyr and 6.6–8.4 kyr B.P. increased by  $>3^\circ\text{C}$  compared with those of other periods (Fig. 6e). This supported the possibility of a southward displacement of the WJ during cold periods. Therefore, the two cold periods in East Asia during the Holocene might have been caused by the southward-shifted WJ. The difference in temperature between the eastern and the western parts of Asia for 6.6–8.4 kyr B.P. might be due to difference in altitude between the western (Tibetan Plateau) and eastern parts of Asia. Generally solar irradiance increases along altitude above sea level (Blumthaler, 2012). In the early Holocene when orbital driven insolation was higher ( $\sim 512 \text{ W/m}^2$ ) than the present level ( $\sim 476 \text{ W/m}^2$ ), the Tibetan Plateau highland region may be more sensitive to surface heating associated with strong insolation compared to the East Asia coastal area. It may cause the relative warming of the highland area, although the East Asia

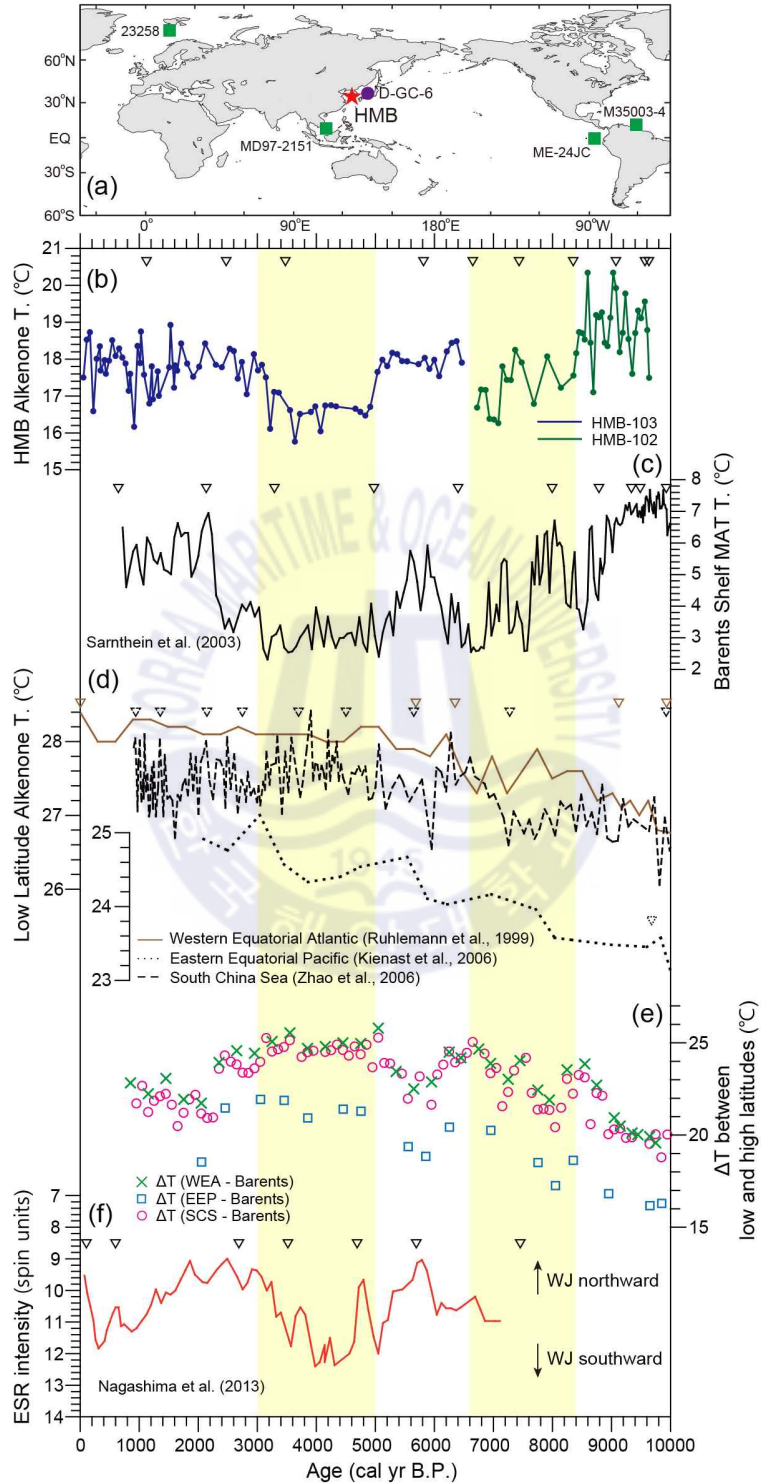


**Fig. 6.** (a) The locations of cores from high- and low-latitudes used in this study. (b) Alkenone-based SST changes in this study. (c) Planktonic foraminiferal MAT-based summer SST changes in the Barents Shelf (Sarnthein et al., 2003). (d) Alkenone-based annual SST changes in the western equatorial Atlantic (Ruhlemann et al., 1999), eastern equatorial Pacific (Kienast et al., 2006), and South China Sea (Zhao et al., 2006). (e) SST gradient between the high-latitude Barents Sea and low-latitude tropics. (f) ESR intensity of silt-sized quartz from core D-GC-6 in the East Sea (Nagashima et al., 2013). Inverted triangle indicates radiocarbon dating.



experienced cooling by the southward migration of the WJ. However, after 5 kyr B.P., insolation decreased ( $\sim 484 \text{ W/m}^2$  at 4 kyr B.P.) and the WJ migrated southward, and these two together caused cooling of both the western and eastern areas.

It was necessary to evaluate the effects of Holocene sea level change and resultant changes in the tidal mixing and ocean current of the Yellow Sea on the variations in the HMB alkenone SST. The magnitude of coastal tidal mixing can be estimated using Eq. (3) (Simpson and Hunter, 1974):

$$\text{Simpson-Hunter index (S)} = \log (H/u^3) \quad (3)$$

where  $H$  is the water depth and  $u$  represents the velocity of the tidal current. Small  $S$  values indicate that tidal mixing becomes active and the SST becomes low (Lie, 1989). Between 7 and 10 kyr B.P., the sea level rose rapidly from  $-40$  to  $-30$  m to its present position (Fig. 7b). A previous study on the reconstruction of the tidal regime changes in the Yellow Sea, based on a two-dimensional tidal model (Uehara and Saito, 2003), demonstrated that the  $u$  values in the study area were almost constant at  $\sim 0.7$  m/s during the entire Holocene. Therefore, variations in  $S$  are solely attributed to the variations in  $H$ . The variation in the water depth of 30–40 m would cause a change in  $S$  of only 0.2 (Fig. 7c). This indicates that the change in the tidal regime during the early Holocene was small. The tidal front that is marked as the boundary between well-mixed regions of shallow water depth and stratified regions of deep water depth generally coincides with Simpson-Hunter parameter ( $S = \log (H/u^3)$ ) value of approximately 2 in the study area (Simpson and Hunter, 1974; Lie., 1989). Since variation in  $S$  distribution was very small ( $\sim 0.2$ ), there appear to be no change in the location of the tidal front. Sea levels remained



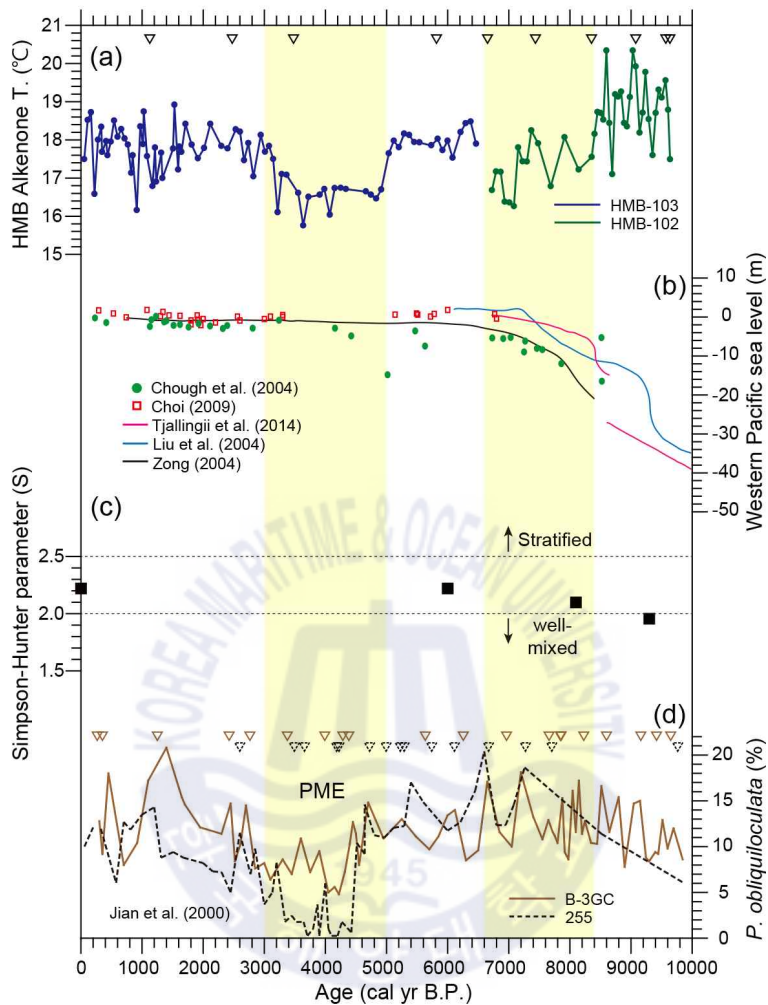


**Fig. 7.** (a) Alkenone-based SST changes in this study. (b) Reconstructed sea-level curves for western Pacific regional seas (Chough et al., 2004; Liu et al., 2004; Zong, 2004; Choi, 2009; Tjallingii et al., 2014). (c) Calculated Simpson-Hunter parameter  $[\log(H/u^3)]$ , which indicates the magnitude of coastal tidal mixing at the location of core HMB-102. (d) Abundance of *P. obliquiloculata* in the Okinawa Trough (Jian et al., 2000). Inverted triangle indicates radiocarbon dating.

constant after 7 kyr B.P. There is little sea level data for the period of 3–5 kyr B.P. (Chough et al., 2004; Choi, 2009) because of an unconformity in the coastal deposits on the west coast of Korea. Choi (2009) suggests that the unconformity might have been caused by the erosion of sediments due to lowering of the sea level. However, even if the sea level lowered, its magnitude might have been much smaller than that in the early Holocene. Therefore, it can be assumed that the change in the  $S$  value at 3–5 kyr B.P. was small and the effects of changes in sea level and tidal mixing on 3–5 kyr B.P. cooling would be insignificant (Fig. 7c).

The inflow of warm Kuroshio branch currents into the shelf area near the Korea Peninsular started between 7 and 8 kyr B.P. when the sea level rose to its present position (Kim and Kucera, 2000; Domitsu and Oda, 2008; Koizumi, 2008; Takata et al., 2019). Yet, the alkenone SST of core HMB-102 decreased from 6.6–8.4 kyr B.P. This might have been because the warm currents were blocked by the tidal front and did not directly flow into the HMB. The spatial distribution of the core-top alkenone SST at 6.5 kyr B.P. (Fig. 3b) showed that the temperature markedly increased southward, corresponding to the shape of the tidal front. According to a recent study in which the trajectories of 433 satellite-tracked drifters, deployed between 1989 and 2004, were analyzed, warm currents do not flow into the study area all year round (Lie and Cho, 2016). In addition, there is an insignificant relationship between the volume transport of the Kuroshio Current and variations in the SST of the Yellow and East China seas between 1982 and 2014 (Kim et al., 2018). Recent studies reported that variations in the SST in this area are associated with changes in atmospheric circulation related to climate variability (Yeh and Kim, 2010; Park et al., 2015). The cold period between 3 and 5 kyr B.P. coincides with the *Pulleniatina* Minimum Event (PME, 2.7–4.6 kyr B.P.) (Fig. 7d; Jian et al., 2000). The PME is characterized

by a low abundance of *P. obliquiloculata*, which is an indicator species of the Kuroshio Current in the Okinawa Trough. Lin et al. (2006) suggest that the abundance of *P. obliquiloculata* reduced during the PME, but what caused the PME remained enigmatic, because there were no significant changes in the Mg/Ca SST and  $\delta^{18}\text{O}$  of seawater (hence salinity) during the PME in the southern Okinawa Trough. Our study suggest that the weakening of the Kuroshio Current did not appear to have caused the cooling of the HMB SST. Instead, the southward-shifted WJ at that time (Fig. 6f) appeared to have caused both cooling of the surface temperature in the mid-latitudes of East Asia and a weakening of the Kuroshio Current. The variations in SST and productivity during the Holocene reconstructed in the northern East China Sea (Wang et al., 2019) showed little changes during the two cold periods 3-5 kyr B.P. and 6.6-8.4 kyr B.P. This difference might be due to different oceanographic settings between the two regions. Upwelling caused by the counterclockwise cold eddy located in the northern East China Sea strongly affects the variation in SST and primary productivity in this region (Yuan et al., 2018; Wang et al., 2019).

## 2.6 Conclusions

The alkenone SSTs have been reconstructed using the alkenone unsaturation index of 81 different core-top sediments from the HMB. Comparison of the core-top alkenone SST with the *in situ* SST, together with the seasonal records of the chlorophyll-a concentration, indicated that the alkenone SST in the study area represented the average SST in April to October. The spatial distribution pattern of the core-top alkenone SST showed that it was generally higher in the south than in the north. This pattern corresponded well with that of the *in situ* SST, indicating that the effects of the resuspension and

lateral transport of sediments on past temperature estimation might be insignificant in this area. The alkenone SST record during the Holocene was reconstructed from the marine sediments of two deep-drilled cores from the HMB. The alkenone SST showed a long-term decrease of 1°C during the entire Holocene. In addition, two long and pronounced cold periods were observed at 3–5 kyr and 6.6–8.4 kyr B.P. in the Holocene. These cold periods were also observed in other regions in the mid-latitudes of East Asia (e.g., Northeast China, lower Yangtze region, Tibetan Plateau), indicating that the cooling pattern was regional. The southward-shifted WJ probably contributed to the pronounced cold periods in East Asia. In contrast, the influence of sea level changes during the Holocene and resultant variations in tidal mixing on the HMB alkenone SST changes was insignificant. The cold period at 3–5 kyr B.P. corresponded with the PME event in the Okinawa Trough, which is characterized by a low abundance of indicator species in the Kuroshio Current. However, it is unlikely that the weakening of the Kuroshio Current directly affected the cooling of the HMB SST. Instead, the southward-shifted WJ seemed to have affected both the cooling of the surface temperature in East Asia and the weakening of the Kuroshio Current.

## Chapter 3.

# Holocene centennial-scale variability in sea surface temperature in the southeast Yellow Sea

### 3.1 Introduction

Variations in solar activity influence the Earth's climate. According to sunspot observations and cosmogenic isotope measurements (e.g.,  $^{14}\text{C}$  in tree-rings and  $^{10}\text{Be}$  in ice cores), solar activity has varied on decadal to millennial timescales during the Holocene (Usoskin, 2017). A general solar cycle (i.e., the Schwabe cycle) lasts 11-years and includes several rises and falls in the number of sunspots (Schwabe, 1843). The polarity of the sunspot magnetic fields changes every two Schwabe cycles. This 22-year magnetic cycle is known as the Hale cycle (Hale, 1919). The amplitude modulation of the Schwabe cycles over a period of ~60–120 years is known as the Gleissberg cycle (Gleissberg, 1939). In addition, longer solar cycles have been previously identified: the 210-year Suess/de Vries (Suess, 1980) associated with the recurrence of Grand minima, the 1,000-year Eddy (Eddy, 1976), and the 2,400-year Hallstatt (Vasiliev and Dergachev, 2002) cycles.

Previous studies have shown that periodic centennial-scale surface temperature changes in East Asia during the Holocene might be induced by solar cycles (Sagawa et al., 2014; Xu et al., 2014; Nan et al., 2017; Park, 2017; Jia et al., 2019). Periods of low surface temperature roughly corresponded to those of weak solar activity. However, the exact relationship between surface temperature and solar activity in this region is not yet clear.

In fact, the resolution of published proxy records is low and spectral analyses have shown that these variables share only 1-2 cyclicities. High-resolution and continuous temporal sea surface temperature (SST) records are needed to clarify the relationship between these parameters.

The degree of unsaturation in C<sub>37</sub> alkenones ( $U_{37}^{k'}$ ) has been widely used as a biomarker for the reconstruction of paleo-SST. The alkenone temperature estimates obtained from 81 core-top sediments recovered from the Heuksan Mud Belt (HMB) (off the southwestern coast of the Korean Peninsula) were compared with *in situ* temperatures. The correspondent results indicated that the alkenone unsaturation index can be used effectively as a proxy for SST in this geographical area (see previous chapter). The study area is characterized by high sedimentation rates (~0.2 cm/year), allowing the reconstruction of the SST record at decadal resolution. Hence, Holocene centennial- to millennial-scale SST variations can be investigated based on the alkenone record. In this study, we reconstructed a high-resolution (10-20 year) SST record covering the last 6.5 kyr B.P. by using the alkenone unsaturation index obtained from marine sediments (from the deep-drilled core HMB-103, recovered from the HMB). Subsequently, we investigated centennial- to millennial-scale SST variability and its relationship with solar activity.

### 3.2 Materials and methods

This study was based on marine sediments samples obtained from the deep-drilled core HMB-103 (Fig. 1b). This core was originally collected in the HMB in 2013 by the Korean Institute of Geoscience and Mineral Resources (KIGAM), using the Chinese drill ship KAN 407. For the alkenone analyses, we used only Holocene muddy sediments collected from the upper 13 m of core HMB-103. The sediment samples were collected at 3 cm intervals in the form

of 1-cm thick slices. As mentioned in the previous chapter, the age of the sediments was estimated by  $^{210}\text{Pb}$  (Park et al., 2000) and through the  $^{14}\text{C}$  analysis of shells and benthic foraminifera (Table 1; Chang and Ha, 2015). The dating results indicate that the sediments of core HMB-103 were deposited during the last 6.5 kyr B.P. The analytical process used for the extraction of alkenones from the sediments was the same described in the previous chapter.

Spectral analyses of the alkenone SST and other proxy records were conducted using the REDFIT 38 software (Schulz and Mudelsee, 2002) with the following parameter settings: Monte Carlo simulations (Nsim) = 1,000, oversampling factor (ofac) = 4, highest frequency factor (hifac) = 1, Welch-overlapped-segment-averaging (WOSA) segment (n50) = 3, and Welch window (Iwin) = 1. A continuous Morlet wavelet transform was performed in MATLAB R2017a using the toolbox of Grinsted et al. (2004). Moreover, a linearly interpolated time series at 10-year intervals was used for the spectral and wavelet analyses.

### 3.3 Results

The high-resolution SST record for the last 6.5 kyr B.P., reconstructed from the sediments of the deep-drilled core HMB-103, is illustrated in Fig. 8a. Along with a long and pronounced cold period between 3–5 kyr B.P., we observed centennial- to millennial- scale fluctuations in the alkenone SST (of maximum  $1^\circ\text{C}$ ). The spectral analysis of alkenone SST revealed significant (>90% confidence level) periodicities of 2,584, 145, 102, 83, and 73 years (Fig. 8b). In order to remove the cooling pattern between 3–5 kyr B.P. and check for periodicities >1,000 years, we extracted the periodicities comprised between 2,000–50 years from the raw dataset by applying a band-pass filter

(Fig. 9a). The spectral analysis of the band-pass filtered alkenone SST data showed that the periodicities of 145, 102, 83, and 73 years identified from the raw data spectrum analysis were still significant (>90% confidence level) (Fig. 9b). Periodicities of 415 and 227 years were also significant, while periodicities >1,000 years were not significant. Overall, the alkenone SST record demonstrated the occurrence of centennial-scale variability over the last 6.5 kyr B.P.





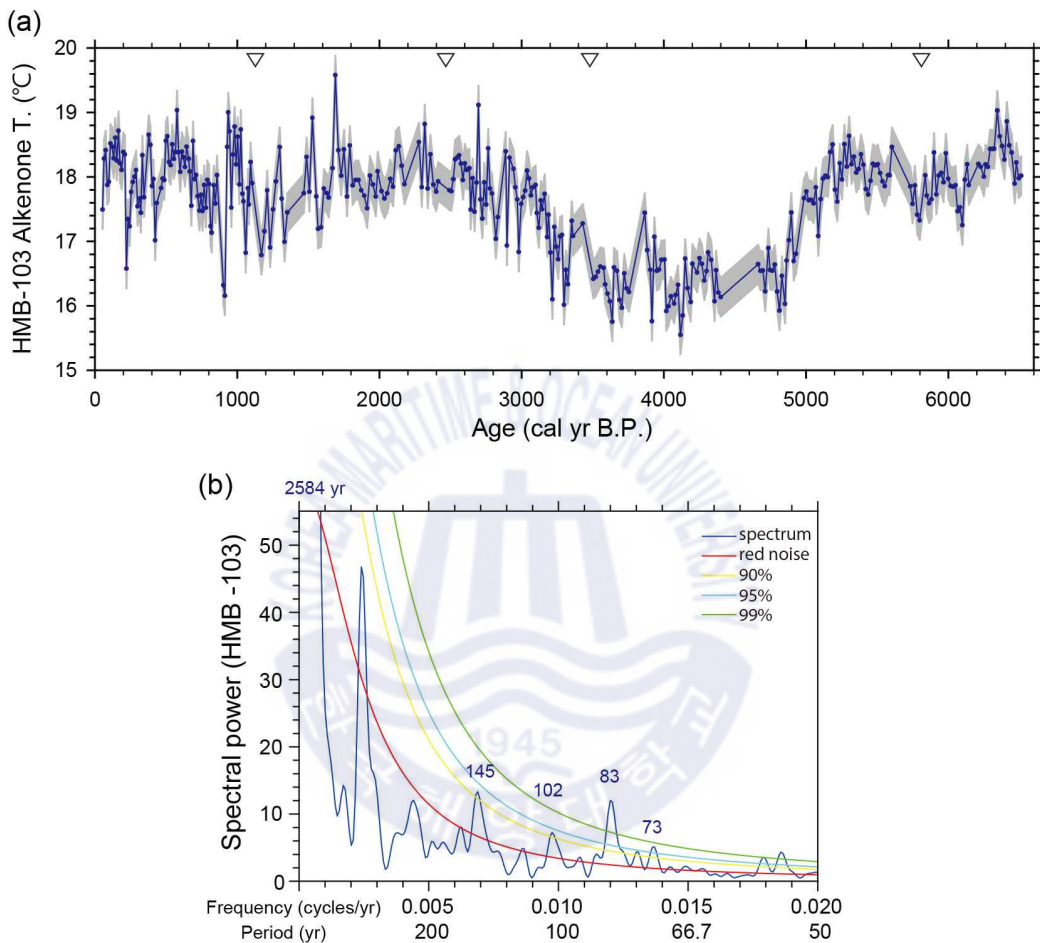


**Fig. 8.** (a) High-resolution alkenone-based SST changes versus calendar age for core HMB-103. Inverted triangles indicate the radiocarbon dates. Gray shading indicates the error range of SST. Inverted triangle indicates radiocarbon dating. (b) Spectral analyses result for HMB-103 alkenone SST (raw data).

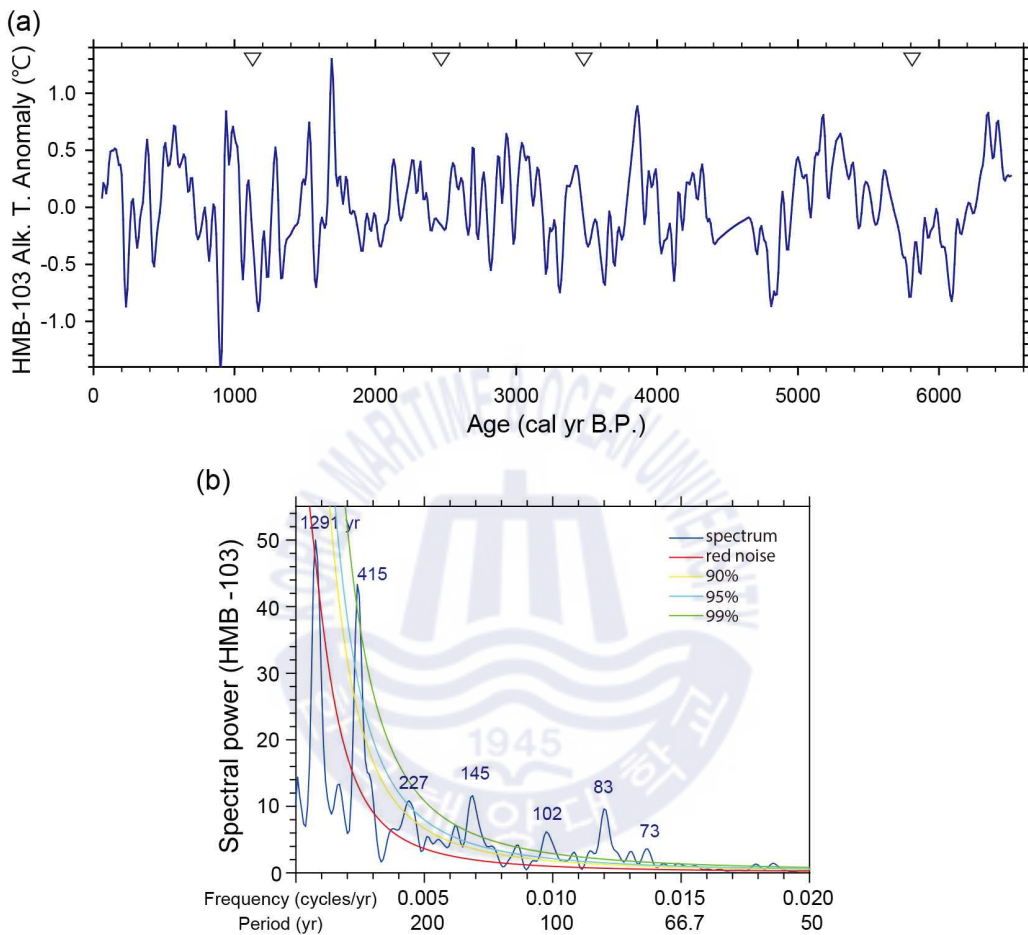


**Fig. 9.** (a) 2000–50 years band-pass filtered HMB-103 alkenone SST, and (b) the result of spectral analyses. Inverted triangle indicates radiocarbon dating.

## 3.4 Discussion

### 3.4.1 Centennial variations in SST and solar activity

To check the accuracy of our age dating, we compared the alkenone-derived SST results obtained from core HMB-103 with those reconstructed from tree ring widths at site JAPA020 (Japan) (Cook et al., 2013; PAGES 2k Consortium, 2013) for the last 2,000 years (Fig. 10). Narrow tree rings were expected to correspond to cold periods. The decreases in alkenone SST were found to be consistent with the tree ring growth index at the centennial scale, highlighting similar trends in the SST and SAT data for the last 2,000 years. These results might also indicate a low age-dating uncertainty, despite the few radiocarbon dates obtained for core HMB-103 (Table 1).

The alkenone SST record obtained from core HMB-103 was compared with the variations in solar activity over the last 6.5 kyr B.P. (Fig. 11a). Total solar irradiance (TSI) data have been previously reconstructed based on the production rates of  $^{10}\text{Be}$ , obtained from ice cores collected in Greenland and Antarctica (Steinhilber et al., 2009). The ages of these ice cores were fairly accurate, since their chronologies were based on annual layer counting. The TSI data obtained from these cores are in good agreement with our SST record at the centennial scale. Periods of low SST correspond approximately to those of low TSI within the estimated age error. In particular, the periods of minimum solar activity known as Dalton (~1820 CE), Maunder (~1680 CE), and Sporer (~1470 CE), which have been previously recognized from sunspot observation data covering the last 500 years, corresponded with those of low SST in our study area.

To further investigate the relationship between alkenone SST and TSI, we

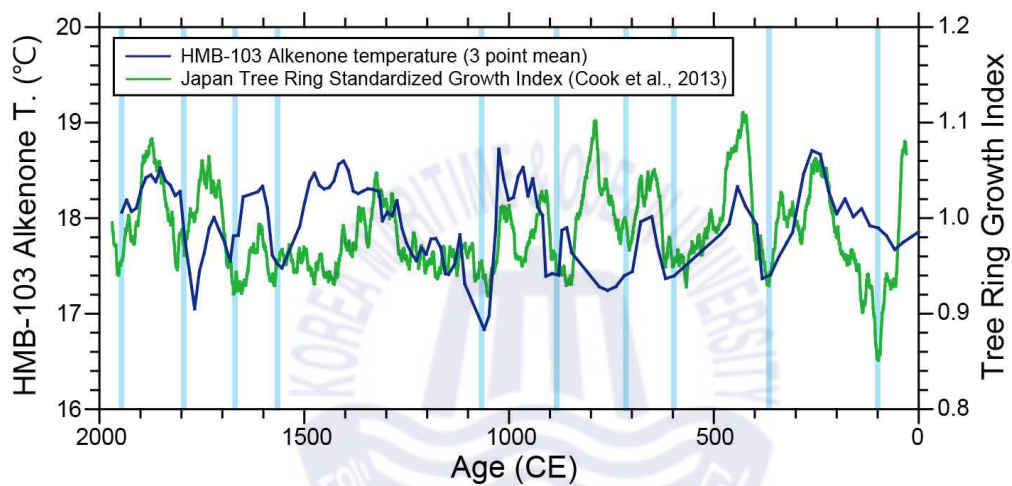
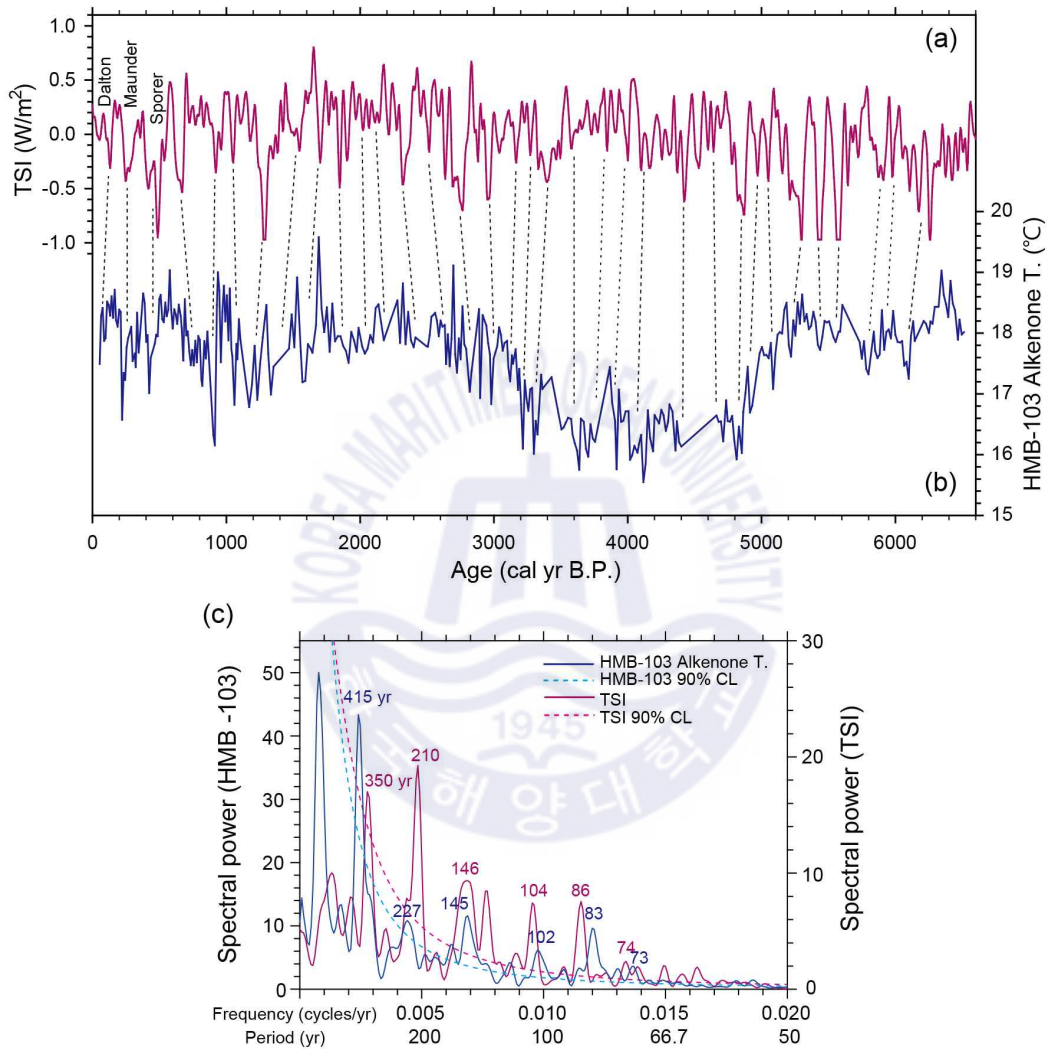


Fig. 10. Comparison of the HMB-103 SST with the tree ring growth index in Japan (Cook et al., 2013) over the last 2000 years.



**Fig. 11.** Comparison of (a) total solar irradiance (TSI) (Steinhilber et al., 2009) with (b) HMB-103 alkenone SST over the last 6.5 kyr B.P. (c) Spectral analyses results for alkenone SST and TSI.

compared the spectrum analysis results obtained from these two datasets and conducted a wavelet coherence analysis (Fig. 11c and 12). The spectral analysis of the TSI revealed that periodicities of 350, 210, 146, 104, 86, and 74 years were significant (>90% confidence level) (Fig. 11b). Cycles of 70–100 years in the HMB-103 alkenone SST record could have been associated with 60–120-year cycles in the TSI record (i.e., Gleissberg cycles) (Usoskin, 2017). Additionally, the 200-year cycles observed in HMB-103 were similar to the 210-year TSI cycles (i.e., Suess/de Vries cycles) (Usoskin, 2017). Finally, the 400-year and 150-year cycles observed in HMB-103 may reflect 350- and 146-year TSI cycles, respectively.

The simultaneous occurrence of low SST and low TSI, combined with the similar cyclicity of alkenone SST and TSI, indicate that the TSI may have influenced the SST centennial-scale variations in the study area.

### 3.4.2 Validation of the centennial-scale SST variations

It has been investigated whether the SST centennial cycles identified in our core were affected by harmonics (e.g., if the observed 145-year cycles in the SST record could have resulted from 73-year harmonics). Periodicities of 100–50, 200–100, 300–200, and 500–400 years were extracted from the 10-year interpolated alkenone SST record by applying a band-pass filter. Then, a spectrum analysis was performed separately (Fig. 13). The results of the spectral analysis on the 100- to 50-year band-pass filtered SST showed that periodicities of 83 and 73 years (previously identified during the raw data spectrum analysis) were still strong (Fig. 13a). In addition, the results of the spectral analysis on the 200- to 100-year band-pass filtered SST showed that periodicities of 145 and 102 years were still significant even after removing the cycles <100 years (Fig. 13b). Likely, the 145-year cycles were not

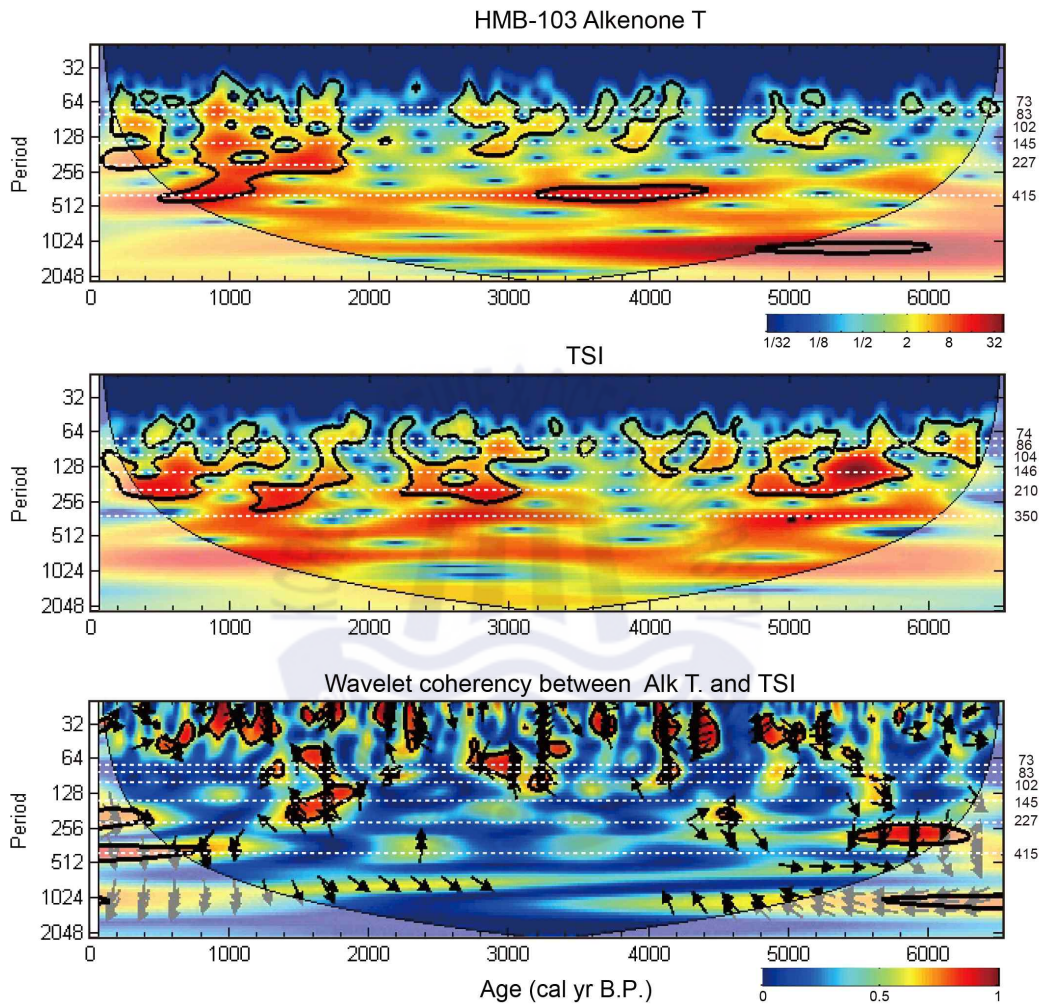
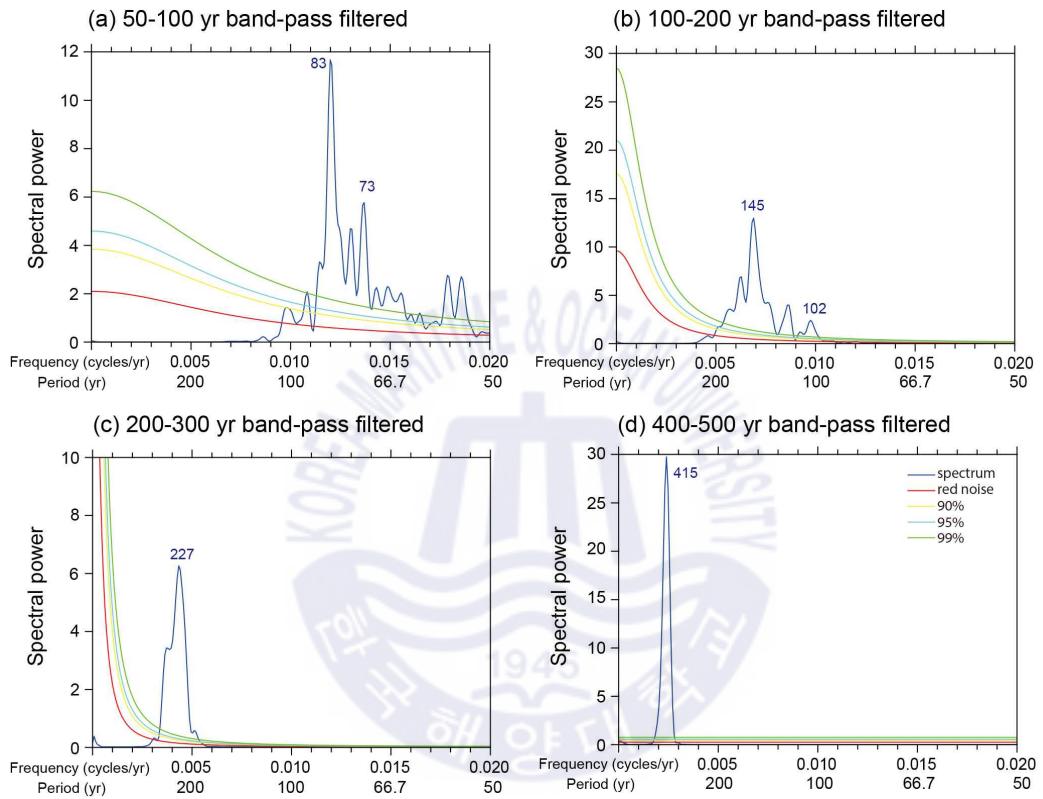


Fig. 12. Continuous transform wavelet spectra for the HMB-103 alkenone SST and TSI, and cross-wavelet spectrum between them.



**Fig. 13.** Spectral analyses results for (a) 100–50 years, (b) 200–100 years, (c) 300–200 years, and (d) 500–400 years band-pass filtered HMB-103 alkenone SST.



affected by 73-year harmonics. The results of the spectral analysis on the 300- to 200-year and 500- to 400-year band-pass filtered SST showed periodicities of 227 and 415 years, respectively (previously identified in the raw data) (Fig. 13c, d). This suggested that all the SST cycles identified in the core were significant and not affected by harmonics.

A previous study demonstrated that solar-type periodicities in high-resolution proxy records might be produced by random variations (Turner et al., 2016). To verify this hypothesis, a series of 15 simple one-dimensional random walks were generated for the last 6.5 kyr B.P. using the R software (RStudio Team, 2015). A spectrum analysis was performed separately (Fig. 14). The random time series of V1 and V11 shared some cyclicity with the alkenone SST record (V1: 406, 147, 104 years; V11: 142, 103, 73 years). However, the periodicities of the other random time series did not match those of the HMB-103 cycles (3 time series matched 1 cycle, while 9 time series did not match any cycle) (Fig. 14). Although the number of random walk simulations was not particularly high, the centennial scale variations in alkenone SST were unlikely to be the product of random variance.

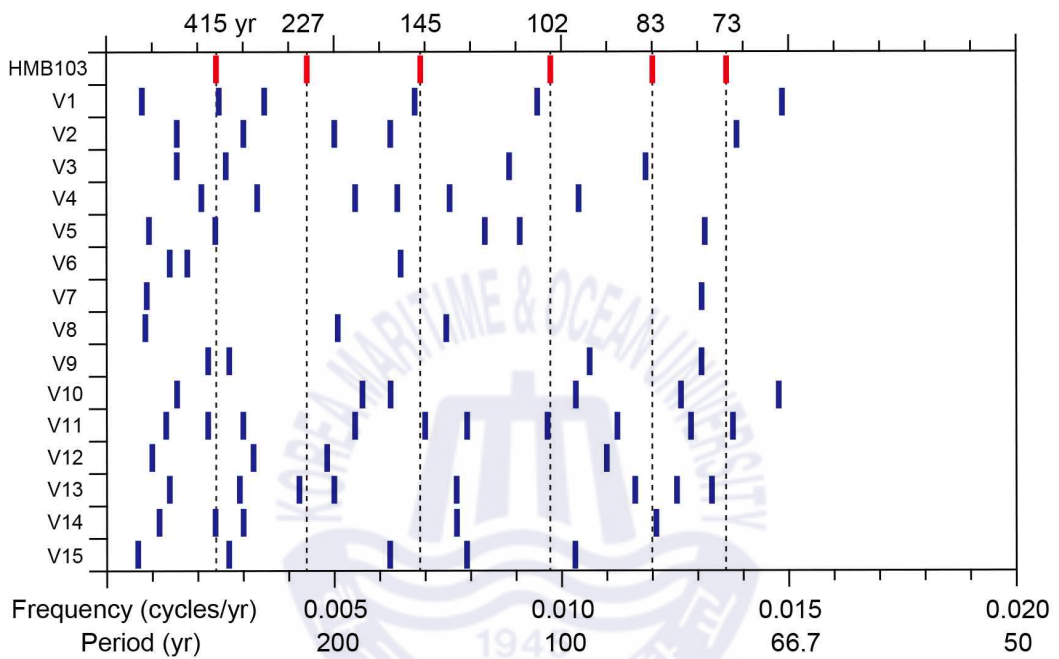
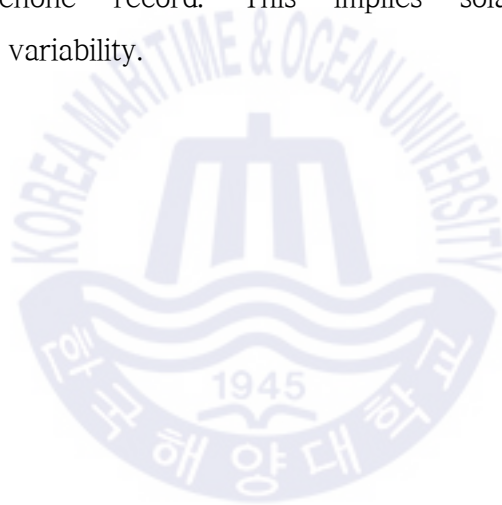


**Fig. 14.** Significant periodicities (>90% confidence level) present in the HMB-103 alkenone SST and 15 random walk simulations.

### 3.5 Conclusions

We obtained a high-resolution SST record (10–20 year) over the last 6.5 kyr B.P. from the marine sediments of deep-drilled core HMB-103. The SST record shows centennial-scale variability. Notably, an overall in-phase relationship is observed between the SST and TSI changes at the centennial-scale. Periods of low SST correspond approximately to those of low TSI within the estimated age error. Solar cycles, such as ~400, 210 (Suess/de Vries cycles), 150, and 120–60 years (Gleissberg cycles), are clearly evident in the HMB-103 Alkenone record. This implies solar forcing of the centennial-scale SST variability.



## Chapter 4. Conclusions

Holocene temperature changes exhibit strong regional patterns. Thus far, the variation in the Holocene temperature of East Asia remains poorly understood owing to limited records. This study reconstructed variations in the SST during the Holocene by using the alkenone unsaturation index of marine sediments of two deep-drilled cores (HMB-102 and HMB-103) that were recovered from the Heuksan mud belt (HMB) located in the southeast Yellow Sea. Alkenone-based temperatures of 81 different surface sediments from the HMB indicates that the reconstructed alkenone temperature from the HMB marine sediments represents the averaged SST from April to October. Our results of alkenone analysis of deep-drilled sediments reveal that there were two long pronounced cold periods at 3–5 kyr B.P. and 6.6–8.4 kyr B.P. during the Holocene. These cold periods were also observed at other mid-latitude regions in East Asia (e.g., Tibetan Plateau, lower Yangtze region, Okinawa Trough), indicating that the cooling pattern was regional. Two cold periods in East Asia seem to be associated with the southward migration of westerly jets. In contrast, the influence of sea level changes during the Holocene and the resultant changes in the tidal mixing and current of the Yellow Sea on SST changes were insignificant.

Superimposed on two long and pronounced cold periods are higher frequency centennial-scale cooling and warming events in the order of  $\sim 1$  °C. The simultaneous occurrence of low SST and low TSI is observed combined with the similar cyclicity of alkenone SST and TSI ( $\sim 400$ , 210 (Suess/de Vries cycles), 150, and 120–60 years (Gleissberg cycles)). This indicates that the TSI may have influenced the SST centennial-scale variations in the study area.

## Acknowledgments

지난 5년 동안의 박사과정 생활을 하면서 정말 많은 분들의 도움과 격려, 조언이 있었습니다. 그분들의 관심이 저를 조금 더 학자다운, 연구자다운 자세를 가질 수 있도록 이끌어 주신 것 같습니다. 아직 부족함이 많습니다. 박사학위가 끝이 아닌 시작이란 생각으로 앞으로 부족한 점을 채우고 제 스스로 단련하여 더욱 발전해 나가는 사람이 되겠습니다.

먼저 박사과정동안 논문을 준비하면서 부족한 저를 지도해주신 이경은 교수님께 감사의 마음을 전하고 싶습니다. 혼자서는 절대 여기까지 오지 못했을 것입니다. 교수님의 헌신적인 가르침과 조언들은 앞으로 제가 어디에서 일을 하든 제 자산이고 밑거름이며 할 수 있다는 용기로 남을 것 같습니다. 진심으로 감사드립니다. 항상 아낌없는 따뜻한 조언을 해주시는 제 공동 지도교수님인 한국해양과학기술원 이희준 박사님께도 감사드립니다. 그리고 논문에 사용한 시료를 획득하고 논문 작성에 많은 도움을 주신 장태수 교수님 감사합니다. 제가 생소한 해양물리분야에서 아낌없는 조언을 해주신 해양과학기술원 박영규 박사님, 전남대학교 최병주 교수님, 한국지질자원연구원 박효석 박사님, 그리고 도기덕 교수님께도 감사의 마음을 전합니다. 바쁘신 와중에도 제 학위논문 심사를 해주시는 부산대학교 함도식 교수님 감사드립니다.

연구실에서 편안하게 조언을 아끼지 않는 지영이 누나, 그리고 항상 성실하게 공부하고 열심히 일하는 태욱이, 령아, 일택이에게도 고맙다는 말을 전하고 싶습니다. 마지막으로 항상 저를 믿고 지켜봐주시는 부모님 감사드립니다.

## References

- Bakker, P., Clark, P.U., Golledge, N.R., Schmittner, A., Weber, M.E., 2017. Centennial-scale Holocene climate variations amplified by Antarctic Ice Sheet discharge. *Nature* 541, 72-76.
- Blumthaler, M., 2012. Solar radiation of the high Alps. In C. Lutz (Ed.), *Plants in alpine regions*. Springer, Wine, New York, pp. 11- 20.
- Bond, G., Kromer, B., Beer, J., Muscheler, R., Evans, M.N., Showers, W., Hoffmann, S., Lotti-bond, R., Hajdas, I., Bonani, G., 2001. Persistent solar influence on North Atlantic climate during the Holocene. *Nature* 294, 2130-2136.
- Chang, T.S., Ha, H.J., 2015. The Heuksan mud belt on the tide-dominated shelf of Korea: a supply-driven depositional system? *Geo-Marine Letters* 35, 447-460.
- Chang, T.S., Ha, H.J., Chun, S.S., 2015. Factors controlling mud accumulation in the Heuksan mud belt off southwestern Korea. *Geo-Marine Letters* 35, 461-473.
- Chen, W., Wang, W.-M., Dai, X.-R., 2009. Holocene vegetation history with implications of human impact in the Lake Chaohu area, Anhui Province, East China. *Vegetation History and Archaeobotany* 18, 137-146.
- Chiang, J.C.H., Fung, I.Y., Wu, C.-H., Cai, Y., Edman, J.P., Liu, Y., Day, J.A., Bhattacharya, T., Mondal, Y., Labrousse, C.A., 2015. Role of seasonal transitions and westerly jets in East Asian paleoclimate. *Quaternary Science Reviews* 108, 111-129.

- Choi, K.H., 2009. Evolution of coastal dune system and sea level change during the Holocene in Korea (Ph. D. diss.). Seoul National University, Seoul, Korea (in Korean).
- Chough, S.K., Lee, H.J., Chun, S.S., Shinn, Y.J., 2004. Depositional processes of late Quaternary sediments in the Yellow Sea: a review. *Geosciences Journal* 8, 211-264.
- Clegg, B.F., Kelly, R., Clarke, G.H., Walker, I.R., Hu, F.S., 2011. Nonlinear response of summer temperature to Holocene insolation forcing in Alaska. *Proceedings of the National Academy of Sciences of the USA* 108, 19299-19304.
- Cook, E.R., Krusic, P.J., Anchukaitis, K.J., Buckley, B.M., Nakatsuka, T., Sano, M., PAGES Asia2k Members, 2013. Tree-ring reconstructed summer temperature anomalies for temperate East Asia since 800 C.E. *Climate Dynamics* 41, 2957-2972.
- Domitsu, H., Oda, M., 2008. Holocene influx of the Tsushima Current into the Japan Sea signalled by spatial and temporal changes in *Neogloboquadrina incompta* distribution. *The Holocene* 18, 345-352.
- Eddy, J.A., 1976. The Maunder minimum. *Science* 192, 1189-1202.
- Gleissberg, W., 1939. A long-periodic fluctuation of the sun-spot numbers. *Observatory* 62, 158-159.
- Grinsted, A., Moore, J.C., Jevrejeva, S., 2004. Application of the cross wavelet transform and wavelet coherence to geophysical time series. *Nonlinear Processes in Geophysics* 11, 561-566.
- Hale, G.E., Ellerman, F., Nicholson, S.B., Joy, A.H., 1919. The magnetic polarity of sun-spots. *Astrophys Journal* 49, 153-178.

- Harada, N., Katsuki, K., Nakagawa, M., Matsumoto, A., Seki, O., Addison, J.A., Finney, B.P., Sato M., 2014. Holocene sea surface temperature and sea ice extent in the Okhotsk and Bering Seas. *Progress in Oceanography* 126, 242-253.
- Herzschuh, U., Borkowski, J., Schewe, J., Mischke, S., Tian, F., 2014. Moisture-advection feedback supports strong early-to-mid Holocene monsoon climate on the eastern Tibetan Plateau as inferred from a pollen-based reconstruction. *Palaeogeography, Palaeoclimatology, Palaeoecology* 402, 44-54.
- Holton, J.R., 2004. An Introduction to Dynamic Meteorology, fourth ed. Elsevier, Boston, MA. 529 pp.
- Hou, J., Huang, Y., Zhao, J., Liu, Z., Colman, S., An, Z., 2016. Large Holocene summer temperature oscillations and impact on the peopling of the northeastern Tibetan Plateau. *Geophysical Research Letters* 43, 1323-1330.
- Jia, Y., Li, D.-W., Yu, M., Zhao, X., Xiang, R., Li, G., Zhang, H., Zhao, M., 2019. High- and low-latitude forcing on the south Yellow Sea surface water temperature variations during the Holocene. *Global and Planetary Change* 182, 103025.
- Jian, Z., Wang, P., Saito, Y., Wang, J., Pflaumann, U., Oba, T., Cheng, X., 2000. Holocene variability of the Kuroshio Current in the Okinawa Trough, northwestern Pacific Ocean. *Earth and Planetary Science Letters* 184, 305-319.
- Jiang, W., Guiot, J., Chu, G., Wu, H., Yuan, B., Hatte, C., Guo, Z., 2010. An improved methodology of the modern analogues technique for palaeoclimate reconstruction in arid and semi-arid regions. *Boreas* 39, 145-153.



- Kienast, M., Kienast, S.S., Calvert, S.E., Eglinton, T.I., Mollenhauer, G., Francois, R., Mix, A.C., 2006. Eastern Pacific cooling and Atlantic overturning circulation during the last deglaciation. *Nature* 443, 846-849.
- Kim, J.-H., Rimbu, N., Lorenz, S.J., Lohmann, G., Nam, S.-I., Schouten, S., Ruhlmann, C., Schneider, R.R., 2004. North Pacific and North Atlantic sea-surface temperature variability during the Holocene. *Quaternary Science Reviews* 23, 2141-2154.
- Kim, J.-M., Kucera, M., 2000. Benthic foraminifer record of environmental changes in the Yellow Sea (Hwanghae) during the last 15,000 years. *Quaternary Science Reviews* 19, 1067-1085.
- Kim, Y.S., Jang, C.J., Yeh, S.-Y., 2018. Recent surface cooling in the Yellow and East China Seas and the associated North Pacific climate regime shift. *Continental Shelf Research* 156, 43-54.
- Ko, T.W., Lee, K.E., Bae, S.W., Lee, S., 2018. Spatial and temporal distribution of C<sub>37</sub> alkenones in suspended materials in the northern East China Sea. *Palaeogeography, Palaeoclimatology, Palaeoecology* 493, 102-110.
- Koizumi, I., 2008. Diatom-derived SSTs (Td' ratio) indicate warm seas off Japan during the middle Holocene (8.2-3.3 kyr BP). *Marine Micropaleontology* 69, 263-281.
- Kong, W., Swenson, L.M., Chiang, J.C.H., 2017. Seasonal transitions and the westerly jet in the Holocene East Asian summer monsoon. *Journal of Climate* 30, 3343-3365.
- Kubota, Y., Kimoto, K., Tada, R., Oda, H., Yokoyama, Y., Matsuzaki, H., 2010. Variations of East Asian summer monsoon since the last deglaciation based on Mg/Ca and oxygen isotope of planktic foraminifera in the northern East China Sea. *Paleoceanography* 25, PA4205.

- Leduc, G., Schneider, R., Kim, J.-H., Lohmann, G., 2010. Holocene and Eemian sea surface temperature trends as revealed by alkenone and Mg/Ca paleothermometry. *Quaternary Science Reviews* 29, 989-1004.
- Lee, C.I., Lee, J.H., Kim, D.S., 2007. Effects of Meteorological Factors on Water Temperature, Salinity in the West Sea of Korea. *Journal of the Korean Society of Marine Environment and Safety* 13, 29-37 (in Korean and English abstract).
- Lee, G.-S., Yoo, D.G., Bae, S.H., Min, G.-H., Kim, S.-P., Choi, H., 2015. Seismic stratigraphy of the Heuksan mud belt in the southeastern Yellow Sea, Korea. *Geo-Marine Letters* 35, 433-446.
- Lee, H.J., Chu, Y.S., 2001. Origin of inner-shelf mud deposit in the southeastern Yellow Sea: Huksan mud belt. *Journal of Sedimentary Research* 71, 144-154.
- Lee, K.E., Lee, S., Park, Y., Lee, H.J., Harada, N., 2014. Alkenone production in the East Sea/Japan Sea. *Continental Shelf Research* 74, 1-10.
- Li, J., Dodson, J., Yan, H., Wang, W., Innes, J.B., Zong, Y., Zhang, X., Xu, Q., Ni, J., Lu, F., 2018. Quantitative Holocene climatic reconstructions for the lower Yangtze region of China. *Climate Dynamics* 50, 1101-1113.
- Li, X., Wang, M., Zhang, Y., Lei, L., Hou, J., 2017. Holocene climatic and environmental change on the western Tibetan Plateau revealed by glycerol dialkyl glycerol tetraethers and leaf wax deuterium-to-hydrogen ratios at Aweng Co. *Quaternary Research* 87, 455-467.
- Lie, H.-J., 1989. Tidal fronts in the southeastern Hwanghae (Yellow Sea). *Continental Shelf Research* 9, 527-546.

- Lie, H.-J., Cho, C.-H., Lee, J.-H., Lee, S., Tang, Y., Zou, E., 2001. Does the Yellow Sea Warm Current really exist as a persistent mean flow? *Journal of Geophysical Research* 106, 22199-22210.
- Lie, H.-J., Cho, C.-H., 2016. Seasonal circulation patterns of the Yellow and East China Seas derived from satellite-tracked drifter trajectories and hydrographic observations. *Progress in Oceanography* 146, 121-141.
- Lin, Y.-S., Wei, K.-Y., Lin, I.-T., Yu, P.-S., Chiang, H.-W., Chen, C.-Y., Shen, C.-C., Mii, H.-S., Chen, Y.-G., 2006. The Holocene *Pulleniatina* Minimum Event revisited: geochemical and faunal evidence from the Okinawa Trough and upper reaches of the Kuroshio Current. *Marine Micropaleontology* 59, 153-170.
- Liu, J.P., Milliman, J.D., Gao, S., Cheng, P., 2004. Holocene development of the Yellow River's subaqueous delta, North Yellow Sea. *Marine Geology* 209, 45-67.
- Marchitto, T.M., Muscheler, R., Ortiz, J.D., Carriquiry, J.D., van Geen, A., 2010. Dynamical Response of the Tropical Pacific Ocean to Solar Forcing During the Early Holocene. *Science* 330, 1378-1381.
- Marcott, S.A., Shakun, J.D., Clark, P.U., Mix, A.C., 2013. A reconstruction of regional and global temperature for the past 11,300 years. *Science* 339, 1198-1201.
- MARGO Project Members, 2009. Constraints on the magnitude and patterns of ocean cooling at the Last Glacial Maximum. *Nature Geoscience* 2, 127-132.
- Marsicek, J., Shuman, B.N., Bartlein, P.J., Shafer, S.L., Brewer, S., 2018. Reconciling divergent trends and millennial variations in Holocene temperatures. *Nature* 554, 92-96.

- Masson-Delmotte, V., Schulz, M., Abe-Ouchi, A., Beer, J., Ganopolski, A., Gonzalez Rouco, J.F., Jansen, E., Lambeck, K., Luterbacher, J., Naish, T., Osborn, T., Otto-Bliesner, B., Quinn, T., Ramesh, R., Rojas, M., Shao, X., Timmermann, A., 2013. Information from Paleoclimate Archives. In: Climate Change 2013: The Physical Science Basis. Contribution of Working Group I to the Fifth Assessment Report of the Intergovernmental Panel on Climate Change [Stocker et al (eds.)]. Cambridge University Press, Cambridge, United Kingdom and New York, NY, USA.
- Nagashima, K., Tada, R., Toyoda, S., 2013. Westerly jet-East Asian summer monsoon connection during the Holocene. *Geochemistry, Geophysics, Geosystems* 14, 5041-5053.
- Nan, Q., Li, T., Chen, J., Chang, F., Yu, X., Xu, Z., Pi, Z., 2017. Holocene paleoenvironment changes in the northern Yellow Sea: evidence from alkenone-derived sea surface temperature. *Palaeogeography, Palaeoclimatology, Palaeoecology* 483, 83-93.
- Pages 2k consortium, 2013. Continental-scale temperature variability during the past two millennia. *Nature Geoscience* 6, 339-346.
- Park, J., 2017. Solar and tropical ocean forcing of late-Holocene climate change in coastal East Asia. *Palaeogeography, Palaeoclimatology, Palaeoecology* 469, 74-83.
- Park, K.-A., Lee, E.-Y., Chang, E., Hong, S., 2015. Spatial and temporal variability of sea surface temperature and warming trends in the Yellow Sea. *Journal of Marine System* 143, 24-38.
- Park, S.-C., Lee, H.-H., Han, H.-S., Lee, G.-H., Kim, D.-C., Yoo, D.-G., 2000. Evolution of late Quaternary mud deposits and recent sediment budget in the southeastern Yellow Sea. *Marine Geology* 170, 271-288.

- Prahl, F.G., Wakeham, S.G., 1987. Calibration of unsaturation patterns in long-chain ketone compositions for palaeotemperature assessment. *Nature* 330, 367-369.
- Prahl, F.G., Muehlhausen, L.A., Zahnle, D.L., 1988. Further evaluation of long-chain alkenones as indicators of paleoceanographic conditions. *Geochimica et Cosmochimica Acta* 52, 2303-2310.
- Qin, Y., Chen, L., Zhao, Y., Zhao, S., 1996. Geology of the East China Sea. Science Press, Beijing, pp. 139-151.
- RStudio Team, 2015. RStudio: Integrated Development for R. RStudio, Inc., Boston, MA URL <http://www.rstudio.com/>.
- Ruhlemann, C., Mulitza, S., Muller, P.J., Wefer, G., Zahn, R., 1999. Warming of the tropical Atlantic Ocean and slowdown of thermohaline circulation during the last deglaciation. *Nature* 402, 511-514.
- Sagawa, T., Kuwae, M., Tsuruoka, K., Nakamura, Y., Ikehara, M., Murayama, M., 2014. Solar forcing of centennial-scale East Asian winter monsoon variability in the mid- to late Holocene. *Earth and Planetary Science Letters* 395, 124-135.
- Sarnthein, M., van Kreveld, S., Erlenkeuser, H., Grootes, P.M., Kucera, M., Pflaumann, U., Schulz, M., 2003. Centennial-to-millennial-scale periodicities of Holocene climate and sediment injections off the western Barents shelf, 75° N. *Boreas* 32, 447-461.
- Schiemann, R., Luthi, D., Schar, C., 2009. Seasonality and interannual variability of the westerly jet in the Tibetan Plateau region. *Journal of Climate* 22, 2940-2957.

- Schulz, M., Mudelsee, M., 2002. REDFIT: estimating red-noise spectra directly from unevenly spaced paleoclimatic time series. *Computers and Geosciences* 28, 421-426.
- Schwabe, H., 1843. Sonnen-Beobachtungen im Jahre 1843. *Astronomische Nachrichten* 21, 233-236.
- Simpson, J.H., Hunter, J.R., 1974. Fronts in the Irish Sea. *Nature* 250, 404-406.
- Steinhilber, F., Beer, J., Frohlich, C., 2009. Total solar irradiance during the Holocene. *Geophysical Research Letters* 36, L19704.
- Stuiver, M., Reimer, P.J., Reimer, R., 2015. CALIB Radiocarbon Calibration Program Revision 7.1. <http://calib.qub.ac.uk/calib/>.
- Suess, H.E., 1980. The radiocarbon record in tree rings of the last 8000 years. *Radiocarbon* 22, 200-209.
- Sun, Y., Oppo, D.W., Xiang, R., Liu, W., Gao, S., 2005. Last deglaciation in the Okinawa Trough: subtropical northwest Pacific link to northern Hemisphere and tropical climate. *Paleoceanography* 20, PA4005.
- Takata, H., Khim, B.-K., Shin, S., Lee, J.-Y., Kim, J.-C., Katsuki, K., Cheong, D., 2019. Early to middle Holocene development of the Tsushima Warm Current based on benthic and planktonic foraminifera in the Nakdong River delta (southeast Korea). *Quaternary International* 519, 183-191.
- Thompson, L.G., Yao, T., Davis, M.E., Henderson, K.A., Mosley-Thompson, E., Lin, P.-N., Beer, J., Synal, H.-A., Cole-Dai, J., Bolzan, J.F., 1997. Tropical climate instability: the last glacial cycle from a Qinghai-Tibetan ice core. *Science* 276, 1821-1825.
- Tjallingii, R., Statterger, K., Stocchi, P., Saito, Y., Wetzels, A., 2014. Rapid flooding of the southern Vietnam shelf during the early to mid-Holocene. *Journal of Quaternary Science* 29, 581-588.

- Turner, T.E., Swindles, G.T., Charman, D.J., Langdon, P.G., Morris P.J. Booth, R.K., Parry, L.E., Nichols, J.E., 2016. Solar cycles or random processes? Evaluating solar variability in Holocene climate records. *Scientific Reports* 6, 23961.
- Uehara, K., Saito, Y., 2003. Late Quaternary evolution of the Yellow/East China Sea tidal regime and its impacts on sediments dispersal and seafloor morphology. *Sedimentary Geology* 162, 25-38.
- Usoskin, I.G., 2017. A history of solar activity over millennia. *Living Reviews in Solar Physics* 14, 1-97.
- Vasiliev, S.S., Dergachev, V.A., 2002. The ~2400-year cycle in atmospheric radiocarbon concentration: bispectrum of  $^{14}\text{C}$  data over the last 8000 years. *Annales Geophysicae* 20, 115-120.
- Wang, Y., Cheng, H., Edwards, R.L., He, Y., Kong, X., An, Z., Wu, J., Kelly, M.J., Dykoski, C.A., Li, X., 2005. The Holocene Asian monsoon: Links to solar changes and North Atlantic Climate. *Science* 308, 854- 857.
- Wang, Z., Xiao, X., Yuan, Z., Wang, F., Xing, L., Gong, X., Kubota, Y., Uchida, M, Zhao, M., 2019. Air-sea interactive forcing on phytoplankton productivity and community structure changes in the East China Sea during the Holocene. *Global and Planetary Change* 179, 80-91.
- Wanner, H., Solomina, O., Grosjean, M., Ritz, S.P., Jetel, M. 2011. Structure and origin of Holocene cold events. *Quaternary Science Reviews* 30, 3109-3123.
- Wanner, H., Mercolli, L., Grosjean, M., Ritz, S.P., 2015. Holocene climate variability and change; a data-based review. *Journal of the Geological Society* 172, 254-263.

- Xu, D., Lu, H., Chu, G., Wu, N., Shen, C., Wang, C., Mao, L., 2014. 500-year climate cycles stacking of recent centennial warming documented in an East Asian pollen record. *Scientific Reports* 4, 3611.
- Yao, T., Thompson, L.G., Mosley-Thompson, E., Zhihong, Y., Xingping, Z., Lin, P.-N., 1996. Climatological significance of  $\delta^{18}\text{O}$  in north Tibetan ice cores. *Journal of Geophysical Research* 101, 29531-29537.
- Yeh, S.-W., Kim, C.-H., 2010. Recent warming in the Yellow/East China Sea during winter and the associated atmospheric circulation. *Continental Shelf Research* 30, 1428-1434.
- Yoo, D.-G., Lee, G.-S., Kim, G.-Y., Kang, N.-K., Yi, B.-Y., Kim, Y.-J., Chun, J.-H., Kong, G.-S., 2016. Seismic stratigraphy and depositional history of late Quaternary deposits in a tide-dominated setting: An example from the eastern Yellow Sea. *Marine and Petroleum Geology* 73, 212-227.
- Yuan, Z., Xiao, X., Wang, F., Xing, L., Wang, Z., Zhang, H., Xiang, R., Zhou, L., Zhao, M., 2018. Spatiotemporal temperature variations in the East China Sea shelf during the Holocene in response to surface circulation evolution. *Quaternary International* 482, 46-55.
- Zhang, D., Feng, Z., 2018. Holocene climate variations in the Altai Mountains and the surrounding areas: A synthesis of pollen records. *Earth-Science Reviews* 185, 847-869.
- Zhang, E., Chang, J., Sun, W., Cao, Y., Langdon, P., Cheng, J., 2018. Potential forcings of summer temperature variability of the southeastern Tibetan Plateau in the past 12 ka. *Journal of Asian Earth Sciences* 159, 34-41.
- Zhang, H., Griffiths, M.L., Chiang, J.C.H., Kong, W., Wu, S., Atwood, A., Huang, J., Cheng, H., Ning, Y., Xie, S., 2018. East Asian hydroclimate

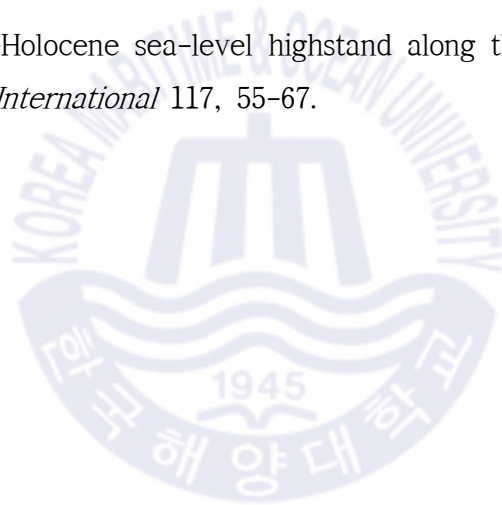


modulated by the position of the westerlies during Termination I. *Science* 362, 580–583.

Zhao, M., Huang, C.-Y., Wang, C.-C., Wei, G., 2006. A millennial-scale sea surface temperature record from the South China Sea (8° N) over the last 150 kyr: monsoon and sea level influence. *Palaeogeography, Palaeoclimatology, Palaeoecology* 236, 39–55.

Zheng, Y., Pancost, R.D., Naafs, B.D.A., Li, Q., Liu, Z., Yang, H., 2018. Transition from a warm and dry to a cold and wet climate in NE China across the Holocene. *Earth and Planetary Science Letters* 493, 36–46.

Zong, Y., 2004. Mid-Holocene sea-level highstand along the southeast coast of China. *Quaternary International* 117, 55–67.



## Appendix A. Supplementary data

### 1. HMB-103 Alkenone SST

No.	Core	section	depth (cm)		calage (yr BP)	Alk. T (°C)
			top	bottom		
1	HMB-103	1	14	15	52	17.5
2	HMB-103	1	29	30	109	18.5
3	HMB-103	1	44	45	165	18.7
4	HMB-103	1	59	60	221	16.6
5	HMB-103	1	74	75	277	18.0
6	HMB-103	1	89	90	333	18.3
7	HMB-103	1	92	93	344	17.7
8	HMB-103	1	110	111	412	18.0
9	HMB-103	1	116	117	434	17.6
10	HMB-103	2	130	131	487	17.9
11	HMB-103	2	145	146	543	18.5
12	HMB-103	2	160	161	599	18.1
13	HMB-103	2	176	177	659	18.3
14	HMB-103	2	190	191	711	18.0
15	HMB-103	2	205	206	767	17.9
16	HMB-103	2	219	220	820	17.1
17	HMB-103	2	226	227	846	17.6
18	HMB-103	3	244	245	913	16.2
19	HMB-103	3	259	260	970	18.3
20	HMB-103	3	271	272	1014	17.9
21	HMB-103	3	274	275	1026	18.7
22	HMB-103	3	289	290	1082	17.6
23	HMB-103	3	307	308	1170	16.8

24	HMB-103	3	313	314	1211	17.8
25	HMB-103	3	316	317	1231	16.9
26	HMB-103	3	328	329	1312	17.7
27	HMB-103	3	331	332	1332	17.0
28	HMB-103	4	357	358	1508	17.8
29	HMB-103	4	360	361	1528	18.9
30	HMB-103	4	369	370	1589	17.2
31	HMB-103	4	372	373	1609	17.8
32	HMB-103	4	377	378	1643	17.7
33	HMB-103	4	387	388	1710	18.4
34	HMB-103	4	402	403	1812	17.9
35	HMB-103	4	417	418	1913	17.5
36	HMB-103	4	432	433	2014	17.8
37	HMB-103	4	447	448	2115	18.4
38	HMB-103	5	474	475	2298	17.8
39	HMB-103	5	489	490	2399	17.8
40	HMB-103	5	513	514	2532	18.3
41	HMB-103	5	528	529	2601	18.2
42	HMB-103	5	543	544	2669	17.5
43	HMB-103	5	558	559	2737	17.9
44	HMB-103	5	576	577	2819	17.0
45	HMB-103	6	603	604	2943	18.1
46	HMB-103	6	618	619	3011	17.7
47	HMB-103	6	633	634	3079	17.8
48	HMB-103	6	647	648	3143	17.5
49	HMB-103	6	663	664	3216	16.1
50	HMB-103	6	678	679	3285	17.1
51	HMB-103	6	695	696	3362	17.1
52	HMB-103	7	734	735	3554	16.6

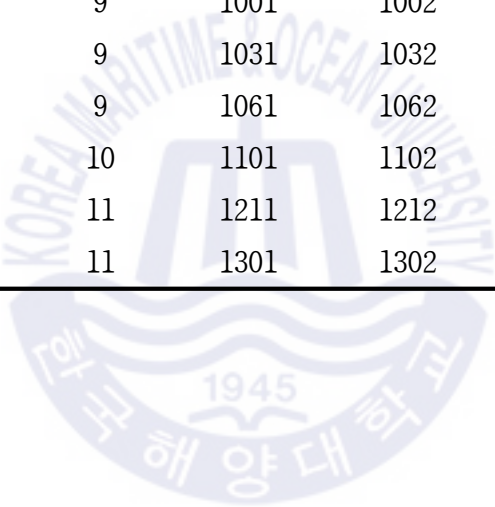
53	HMB-103	7	749	750	3638	15.8
54	HMB-103	7	764	765	3721	16.5
55	HMB-103	8	797	798	3905	16.6
56	HMB-103	8	811	812	3983	16.7
57	HMB-103	8	827	828	4072	16.0
58	HMB-103	8	841	842	4150	16.7
59	HMB-103	8	859	860	4250	16.7
60	HMB-103	8	874	875	4334	16.7
61	HMB-103	9	933	934	4662	16.6
62	HMB-103	9	948	949	4746	16.6
63	HMB-103	9	963	964	4829	16.5
64	HMB-103	9	978	979	4913	16.7
65	HMB-103	10	1000	1001	5035	17.6
66	HMB-103	10	1015	1016	5119	18.0
67	HMB-103	10	1030	1031	5202	17.8
68	HMB-103	10	1045	1046	5286	18.2
69	HMB-103	10	1060	1061	5369	18.1
70	HMB-103	10	1075	1076	5453	17.9
71	HMB-103	10	1090	1091	5537	17.9
72	HMB-103	11	1125	1126	5731	17.9
73	HMB-103	11	1144	1145	5837	18.0
74	HMB-103	11	1158	1159	5915	17.7
75	HMB-103	11	1173	1174	5999	18.0
76	HMB-103	11	1188	1189	6082	17.5
77	HMB-103	12	1211	1212	6210	18.2
78	HMB-103	12	1226	1227	6294	18.4
79	HMB-103	12	1241	1242	6377	18.5
80	HMB-103	12	1257	1258	6467	17.9

## 2. HMB-102 Alkenone SST

No.	Core	section	depth (cm)		calage (yr BP)	Alk. T (°C)
			top	bottom		
1	HMB-102	5	511	512	6727	16.7
2	HMB-102	5	520	521	6791	17.2
3	HMB-102	5	531	532	6870	17.2
4	HMB-102	5	540	541	6934	16.4
5	HMB-102	5	551	552	7012	16.4
6	HMB-102	5	561	562	7084	16.3
7	HMB-102	5	571	572	7155	17.8
8	HMB-102	5	581	582	7227	17.4
9	HMB-102	5	591	592	7298	17.4
10	HMB-102	6	601	602	7370	18.2
11	HMB-102	6	612	613	7480	17.9
12	HMB-102	6	621	622	7687	16.8
13	HMB-102	6	631	632	7917	18.1
14	HMB-102	6	641	642	8147	17.2
15	HMB-102	6	651	652	8359	17.5
16	HMB-102	6	661	662	8407	18.2
17	HMB-102	6	671	672	8455	18.7
18	HMB-102	6	681	682	8504	18.7
19	HMB-102	6	691	692	8552	18.5
20	HMB-102	6	701	702	8600	20.3
21	HMB-102	6	711	712	8648	18.4
22	HMB-102	7	721	722	8697	17.1
23	HMB-102	7	731	732	8745	19.2
24	HMB-102	7	741	742	8793	19.1
25	HMB-102	7	751	752	8841	19.3
26	HMB-102	7	761	762	8890	18.4

27	HMB-102	7	771	772	8938	18.3
28	HMB-102	7	781	782	8986	19.1
29	HMB-102	7	791	792	9035	20.3
30	HMB-102	7	801	802	9080	19.9
31	HMB-102	8	841	842	9145	18.2
32	HMB-102	8	871	872	9194	18.7
33	HMB-102	8	898	899	9239	19.8
34	HMB-102	8	931	932	9293	18.5
35	HMB-102	9	971	972	9358	17.6
36	HMB-102	9	1001	1002	9408	18.7
37	HMB-102	9	1031	1032	9457	19.3
38	HMB-102	9	1061	1062	9506	19.1
39	HMB-102	10	1101	1102	9570	19.6
40	HMB-102	11	1211	1212	9611	18.8
41	HMB-102	11	1301	1302	9644	17.5

---



### 3. Core-tops Alkenone SST

No.	Core		depth (cm)		location		Alk. T (°C)
			top	bottom	longitude (°E)	latitude (°N)	
1	12HMB	P01	0	1	125.92	33.75	18.1
2	12HMB	P02	0	1	125.81	33.71	19.4
3	12HMB	P04	0	1	125.69	33.81	19.4
4	12HMB	P05	0	1	125.63	33.91	18.3
5	12HMB	P06	0	1	125.67	33.92	17.9
6	12HMB	P07	0	1	125.71	33.93	18.6
7	12HMB	P08	0	1	125.84	33.97	16.9
8	12HMB	P09	0	1	125.73	34.06	18.1
9	12HMB	P10	0	1	125.66	34.04	18.0
10	12HMB	P11	0	1	125.57	34.02	18.1
11	12HMB	P12	0	1	125.54	34.14	17.9
12	12HMB	P13	0	1	125.62	34.16	18.1
13	12HMB	P14	0	1	125.57	34.28	17.7
14	12HMB	P15	0	1	125.34	34.21	17.7
15	12HMB	P16	0	1	125.49	34.49	17.6
16	12HMB	B01	0	1	125.93	33.64	22.1
17	12HMB	B02	0	1	126.02	33.66	21.2
18	12HMB	B03	0	1	126.09	33.68	21.3
19	12HMB	B04	0	1	126.20	33.65	21.2
20	12HMB	B05	0	1	125.74	33.70	21.4
21	12HMB	B06	0	1	125.87	33.73	20.3
22	12HMB	B07	0	1	125.97	33.76	19.1
23	12HMB	B08	0	1	126.03	33.83	19.4
24	12HMB	B09	0	1	125.82	33.85	18.4
25	12HMB	B10	0	1	126.00	33.90	19.4
26	12HMB	B11	0	1	126.17	33.95	20.3

27	12HMB	B12	0	1	125.96	33.91	18.8
28	12HMB	B13	0	1	125.53	33.88	19.2
29	12HMB	B15	0	1	125.90	33.96	19.0
30	12HMB	B16	0	1	126.02	34.02	20.1
31	12HMB	B17	0	1	125.85	34.02	17.7
32	12HMB	B18	0	1	125.45	33.98	18.1
33	12HMB	B19	0	1	125.52	34.00	18.7
34	12HMB	B20	0	1	125.80	34.09	17.2
35	12HMB	B22	0	1	125.39	34.09	18.5
36	12HMB	B23	0	1	125.48	34.12	18.9
37	12HMB	B24	0	1	125.75	34.20	17.0
38	12HMB	B25	0	1	125.74	34.21	18.2
39	12HMB	B26	0	1	125.76	34.29	18.3
40	12HMB	B27	0	1	125.29	34.20	18.3
41	12HMB	B28	0	1	125.52	34.26	18.1
42	12HMB	B29	0	1	125.64	34.30	18.6
43	12HMB	B30	0	1	125.80	34.35	18.5
44	12HMB	B31	0	1	125.67	34.38	16.9
45	12HMB	B32	0	1	125.52	34.40	17.3
46	12HMB	B33	0	1	125.64	34.45	17.6
47	12HMB	B34	0	1	125.60	34.55	17.6
48	12HMB	B35	0	1	125.44	34.60	18.2
49	13HMB	P01	0	1	125.79	33.71	18.7
50	13HMB	P02	0	1	126.05	33.67	20.2
51	13HMB	P03	0	1	126.10	33.68	19.3
52	13HMB	P04	0	1	126.17	33.64	20.5
53	13HMB	P05	0	1	126.19	33.63	21.4
54	14HMB	P01	0	1	125.81	34.25	17.7
55	14HMB	P02	0	1	125.87	35.33	17.5



56	14HMB	P03	0	1	125.94	35.42	16.5
57	14HMB	P04	0	1	125.82	35.17	16.3
58	14HMB	P05	0	1	125.71	35.08	17.3
59	14HMB	P06	0	1	125.66	35.00	17.9
60	14HMB	P07	0	1	125.67	34.92	17.3
61	14HMB	P08	0	1	125.67	34.83	18.4
62	14HMB	P09	0	1	125.69	33.93	17.7
63	14HMB	P10	0	1	125.69	33.93	17.9
64	14HMB	B01	0	1	125.75	34.75	17.4
65	14HMB	B02	0	1	125.75	34.83	18.1
66	14HMB	B03	0	1	125.58	34.83	17.1
67	14HMB	B04	0	1	125.58	34.92	17.2
68	14HMB	B05	0	1	125.58	35.00	17.6
69	14HMB	B06	0	1	125.58	35.08	17.4
70	14HMB	B07	0	1	125.59	35.17	16.8
71	14HMB	B08	0	1	125.67	35.25	16.8
72	14HMB	B09	0	1	125.71	35.33	17.4
73	14HMB	B10	0	1	125.86	35.42	17.4
74	14HMB	B11	0	1	126.10	35.42	16.2
75	HMB	V01	0	1	125.69	33.98	18.5
76	HMB	V02	0	1	125.37	34.09	18.1
77	HMB	V03	0	1	125.37	34.22	19.2
78	HMB	V04	0	1	125.45	34.57	17.7
79	HMB	V05	0	1	125.61	34.60	18.5
80	HMB	V06	0	1	125.82	33.65	19.6
81	HMB	V07	0	1	125.62	34.16	18.2